University of Southern Queensland

Faculty of Health, Engineering and Sciences

Analysis on the Behaviour of FRP Reinforced Concrete Railway Sleepers

A dissertation submitted by

Trent Baker

in fulfilment of the requirements of

ENG4111 and 4112 Research Project

towards the degree of

Bachelor of Engineering (Honours) (Civil)

Submitted October, 2016

ABSTRACT

The most commonly used materials for railway sleepers include timber, steel and concrete; with each of these materials possessing different characteristics that leave them susceptible to various failure modes. Due to this many sleepers fail before they reach their target design life, which is estimated to cost the Australian Railway Industry up to $80 million per year, therefore highlighting the need for a more durable sleeper design. This dissertation assesses the potential of concrete railway sleepers reinforced glass fibre reinforced polymer (GFRP) bars as a solution to this problem.

The dissertation involved analysing the current proposed pressure distribution patterns under the sleeper for varied ballast conditions, to determine which assumed pressure distribution gave the most critical design forces. With the critical patterns determined the effect of key sleeper parameters of support modulus and sleeper modulus were then evaluated. The results indicated that the bearing pressure distribution had a significant effect on the design forces, while the other parameters' effects were negligible.

With the critical design forces and corresponding parameters determined the required reinforcement layout for a narrow gauge concrete sleeper for both steel and GFRP bars were calculated. A finite element model was then developed for both alternative reinforcement materials, to compare and evaluate the performance of the new GFRP reinforced sleeper against a traditional steel reinforced concrete sleeper.

From the results it was concluded that the concrete sleeper reinforced with GFRP bars performs just as well as the steel reinforced sleeper, but due to the lower modulus of elasticity for GFRP compared to steel, this design requires a significantly larger percentage of reinforcement (approximately 50%) to meet serviceability requirements. Therefore, further work needs to be undertaken to determine if there is an overall cost benefit in adopting this new design.

Certification

I certify that the ideas, designs and experimental work, results, analyses and conclusions set out in this dissertation are entirely my own effort, except where otherwise indicated and acknowledged.

I further certify that the work is original and has not been previously submitted for assessment in any other course or institution, except where specifically stated.

Trent Baker

Student Number: 0061046529

ACKNOWLEDGEMENTS

I would like to acknowledge the following people:

Dr Allan Manalo for his invaluable guidance and support throughout the preparation of this dissertation.

Also I would like to thank my family and friends for their ongoing support and encouragement throughout my studies.

Table of Contents

List of Figures

List of Tables

Nomenclature and Acronyms

GFRP	-	Glass Fibre Reinforced Polymer
FRP	-	Fibre Reinforced Polymer
MPa	-	Mega Pascals
GPa	-	Giga Pascals
kN	-	Kilo-Newton
mm	-	Millimetres
DEF	-	Delayed Ettringite Formation
AAR	-	Alkali-Aggregate Reaction
ROA	-	Railway of Australia
FEM	-	Finite Element Model
FEA	-	Finite Element Analysis
AUD	-	Australian Dollars
BTM	-	Bottom

CHAPTER 1 INTRODUCTION

1.1   Background

The safety and reliability of railways as a mode of transportation is dependent on the quality of the railway track system and each of its components, in particular the railway sleepers. The sleepers are the beams laid underneath the rail tracks, which as explained by Zhao, Chan and Burrow (2006) serve the function of transferring and distributing the loads of the rail to the ballast, transversely securing the rails at the correct gauge, resisting cutting and abrading actions of the bearing plates and the ballast and preventing lateral and longitudinal movement of the track.

Timber, steel and concrete are the main materials used for railway sleepers, with target life spans of 20, 50 and 50 years respectively. A large number of these traditional sleepers, even with perfect support conditions, do not reach their target life due to unexpected failure modes. It is estimated that the Australian railway industry could reduce its operating cost by up to $80 million per annum by improving its operation and maintenance procedures (Ferdous and Manalo, 2014).

While prestressed steel reinforced concrete sleepers possess characteristics that make it more suitable as a sleeper material compared to timber and steel, this alternative is still vulnerable to different failure modes. The major failure modes include: rail seat deterioration, centre-bound damage, derailment, high impact loading, delayed ettringite formation (DEF), Alkali-Aggregate reaction (AAR), acid attack in concrete, ice forming in sleepers. These failure modes all lead to cracking of the sleeper and/or deterioration of the concrete cover which then leaves the sleeper susceptible to bar corrosion and ultimately early failure.

This highlights the need for a solution to the current sleeper maintenance issue. Therefore, this research will assess the potential of concrete railway sleepers reinforced with glass fibre reinforced polymer (GFRP) bars, as a potential solution to this problem.

1.2   Aims and Objectives

GFRP bars possess superior corrosion resistant properties and are a light weight alternative to steel reinforcement. These qualities make concrete sleepers reinforced with GFRP bars a potential solution to the current railway sleeper maintenance problem being experienced around the world. As a part of the assessment of the potential of this new design this project will aim to complete the following tasks:

- Research background information on the design and analysis of concrete railway sleepers.

- Compare and evaluate the existing equations and theories for calculating the maximum positive and negative bending moment and shear forces that the sleepers are subjected to, using theoretical and Finite Element Modelling (FEM) analyses.

- Perform parametric investigations utilising either theoretical or FEM analysis to determine the effect of important design parameters on the behaviour of precast concrete sleepers and evaluate against the performance requirements for a Queensland precast concrete railway sleeper.

- Evaluate the structural behaviour of the precast concrete sleeper reinforced with GFRP bars and compare with the performance of an existing precast concrete sleeper reinforced with steel reinforcement, using FEM simulation.

The scope of this undergraduate project restricts the analysis of the new concrete sleeper to only the basic structural behaviour of the design, including load-deflection, flexural and shear strength. Due to the nature of the project and time and resource limitations other characteristics of the design such as its durability and the effects of temperature and fatigue due to the cyclic loading on the sleeper were not considered.

1.3   Expected Outcomes and Benefits

Although GFRP reinforced concrete structures are becoming more common in the construction industry, this reinforcing technology is yet to be applied to concrete railway sleepers. Therefore, this project is being undertaken to investigate the potential of pre cast concrete railway sleepers reinforced with GFRP bars. The success of this design could

potentially provide a solution to the timber sleeper replacement issues currently being experienced by the railway industries.

The expected outcomes of the project are:

- To determine equations/theories that can accurately calculate the bending moment and shear force that the concrete sleepers reinforced with GFRP bars will be subjected to.

- To determine which sleeper bearing pressure distribution most accurately represents the current methods employed by the Australian prestressed concrete sleeper standard.

- To determine the effects of concrete strength and arrangement of GFRP bars on the structural behaviour of the sleeper.

- A comparison between the performance of the proposed new design and existing steel reinforced concrete sleepers.

The information determined from this project could highlight the potential for further research on this topic. Successful development of this sleeper design could provide benefits for railway industries all around the world.

CHAPTER 2   LITERATURE REVIEW

2.1   Background on Railway Sleepers

Rail plays an important role in the transportation of both people and products around the world, with many industries, especially the Australian mining industry heavily relying on this form of transportation. It is reported that in 1998 the Australian railway industry spent approximately 25-35 percent of its annual budget on track maintenance with sleeper replacement accounting for a significant portion of this (Remennikov and Kaewunruen 2005). This highlights the fact that there needs to be improvements made in certain aspects of the design of sleepers in particular durability.

The most common type of railway track used in Australia is the ballasted railway. In a ballasted railway the forces induced by the train are directed from the rails into the sleepers which then transfer the loading through the ballast and into the subgrade (Precast Concrete Railway Track Systems, 2006). A Typical ballasted railway cross section can be seen in Figure 2.1 below. This type of system is split into two structures, these being the super-structure and the sub-structure. The super-structure consists of the rails, the fastening systems and the sleeper, while the sub-structure consists of the ballast, sub-ballast and the subgrade (Remennikov and Kaewunruen 2005).
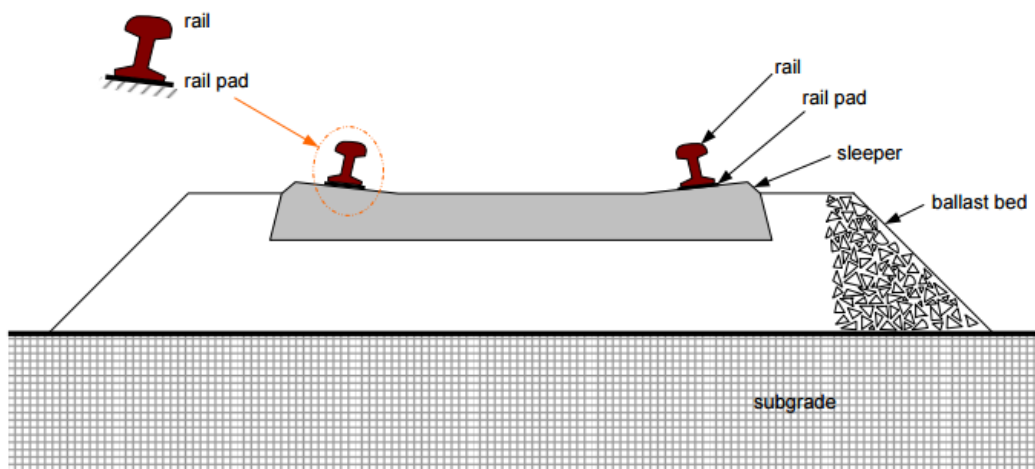
Figure 2.1: Typical ballasted track structure (Remennikov and Kaewunruen 2005)

Some of the advantages of ballasted track compared to non-ballasted track include (Precast Concrete Railway Track Systems, 2006):

- Lower initial construction costs.

- Lower noise levels due to the ballast absorbing some noise.

- Lower difficulty and cost to repair track damage.

- Shorter construction time.

As can be seen from figure 2.1 the sleepers are transverse structural members which are placed on top of the ballast and support the rails. As explained by Remennikov and Kaewunruen (2005), railway sleepers were initially made from timber and then from steel for limited applications and now the majority of sleepers used in Australian railway tracks are made of prestressed concrete. Jeffs and Tew (1991) highlighted in their research that in 1986 Australia had approximately 77 million sleepers making up the countries 49,000 km of railway track, with 84% of these sleepers made of timber, 15% from concrete and 1% made of steel. At this time the number of sleepers being replaced each year was around 3,000,000 timber, 500,000 concrete and 250,000 steel sleepers (Hansard, 1988). Due to the large increase in the popularity of concrete sleepers in Australian railway track since this time it is reasonable to assume that the number of concrete sleepers being replaced each year would be in the millions.

As adapted from Remennikov and Kaewunruen (2005) the main functions of the sleepers are to:

- Support and restrain the rail

- Transfer loads from the rail to the supporting ballast

- Maintain the rail gauge and inclination

- Withstand lateral, longitudinal and vertical rail movements

- Maintain resistance to wearing and loading throughout changes in temperature and weather conditions

The type of sleeper considered in this project will be a mono block concrete sleeper. Concrete sleepers come in two main types – reinforced twin block sleepers and prestressed mono block sleepers. Twin block sleepers are commonly used around the world on standard lines for 25tonne axle loads up to speeds of 200km/hr while mono block sleepers are used throughout the world for all types of rail lines, especially heavy haul lines with axle loads of up to 35 tonnes (Precast Concrete Railway Track Systems, 2006).

2.2 Failure Modes of Sleepers

Due to the decreasing availability of natural resources for production of new sleepers and the increasing costs involved with replacement of sleepers, it is clear that the failure mechanisms of sleepers need to be understood and alternative designs developed. It has been reported that the Australian railway industry could potentially save $80 million AUD in annual expenses by improving on the current railway operation and maintenance procedures (Morris et al 1995). The results of a survey on the sleepers used throughout the world's railway networks performed by the International Federation for Structural Concrete (2006), are presented in table 2.1.

Table 2.1: Sleepers used throughout the world's railway networks (adopted from Ferdous and Manalo 2014)

Country	Total sleepers in track (×1000)	Demands per year (×1000)		
		Concrete	Steel	Timber
Argentina	–	60	–	–
Australia	600,000	–	150	200
Austria	9000	200	70	100
Belgium	9912	400	2	20
Brazil	50,000	500	60	300
Chile	5300	200	–	–
China	115,000	3000	–	–
Colombia	5080	–	–	–
Czech Rep.	17,000	250	–	3
Denmark	–	150	–	–
France	60,000	800	0	400
Germany	70,000	1400	100	100
Greece	6150	30	5	3
Hungary	20,388	–	–	–
India	163,500	4640	–	–
Italy	40,000	2000	–	–
Japan	34,000	400	–	–
Malaysia	3000	–	–	–
Morrocco	5000	–	–	–
Netherlands	8500	400	–	–
Norway	3000	60	–	–
Romania	16,000	12	–	–
Russia	150,000	3500	–	–
S. Africa	43,000	305	0	0
Spain	30,000	1200	0	30
Sweden	19,500	400	–	8
Switzerland	17,000	150	–	–
Taiwan	4000	120	0	12
USA	600,000	1000	10	13,000
UK	45,000	500	400	100
Venezuela	1225	–	–	–

From Table 2.1 it is clear that concrete sleepers are the most commonly used material throughout the majority of countries around the world and that the major focus of development of new sleeper design and maintenance strategies should focus on concrete

sleeper failure mechanisms. This is supported by Palomo et al (2007), who reported that there are over 400 million concrete sleepers throughout the world's railway networks, with 2 – 5% needing replacement each year. Due to these findings this section will only briefly cover timber and steel failure mechanisms and focus in detail on concrete sleepers.

2.2.1   Timber sleeper failure

There are number of different causes of failure in timber sleepers, with some more common than others depending on the loading set up and the surrounding environmental conditions. As explained by Ferdous and Manalo (2014), the Railway of Australia (ROA) (1991) performed a survey on 2200 timber sleepers in Queensland Railway tracks to identify the main cause of damage to the timber sleepers. The results of this survey showed that there were a number of different causes of damage including fungal decay, end splitting, termites, still sound, sapwood, shelling, rail cut, weathering, spike kill and knots. From the survey it was found that fungal decay, end splitting and termite attacks were the most encountered causes of damage with 53%, 10%, 7% of the overall damage modes respectively.

2.2.2   Steel sleeper failure

Steel has a number of characteristics which make it problematic as a sleeper material; hence there has been limited application of steel sleepers in mainline railway tracks throughout the world. These characteristics identified by Ferdous and Manalo (2014), include the high risk of corrosion, high electrical conductivity, fatigue cracking and due to the difficulties that arise in trying to pack steel sleepers with ballast. It was explained in this study that corrosion in steel sleepers can occur due to the contact with salty elements which can come from soil, groundwater and aggregates while fatigue cracking can occur as a result of the cyclic loading at the rail seat due to the passing train.

2.2.3   Concrete Sleeper failure

While concrete has many characteristics that make it more suitable for use as a sleeper material compared to steel and timber, it is still vulnerable to different types of failure. The main types of failure that occur are rail seat deterioration, Centre-bound damage, derailment, high-impact loading, delayed ettringite formation (DEF), Alkali- aggregate reaction (AAR), acid attack in concrete, bar corrosion and ice forming in the sleeper.

Rail seat deterioration is the most commonly occurring failure mode for concrete sleepers for many different countries around the world (Ferdous and Manalo 2014). According to

Bakharev and Struble (1997) this type of failure is generally caused by rail-seat abrasion but can also be due to hydro abrasive erosion, hydraulic pressure cracking, freeze thaw cracking or chemical deterioration.

Centre-bound damage occurs due to heavy loading causing tensile fractures in the sleeper. Studies by González-Nicieza et al (2008) and Rezaie et al (2012) both report on clear examples of centre-bound damage, with the former finding failure by vertical cracking caused by tensile cracking and the latter finding longitudinal cracking caused by tensile fracture.

As reported by Ferdous and Manalo (2014) derailment is caused by defects in the sleepers which generally occur throughout the operational stages due to manpower faults and defects in the track. This is considered the worst case of failure as derailment can cause series harm or loss of life and requires expensive repair work before the track can be reopened.

The next common concrete sleeper failure mode is due to High-impact loading. This high-impact loading is caused by either wheel flats or dipped rails, which is not considered in current design methods. This high loading can therefore induce loads higher than were considered for the design and can cause cracking of the sleeper, generally at the sleeper centre (Ferdous and Manalo 2014).

Delayed ettringite formation is another type of failure mode that can cause concrete railway sleepers to fail before they reach their intended design life. This type of failure occurs when either soil, groundwater or aggregates containing sulfates of sodium, potassium, magnesium and calcium react with the tricalcium aluminate or calcium hydroxide in the cement paste causing expansion and eventually cracking of the concrete which can lead to complete failure (Narayanan and Beeby 2005 and Neville 2012). The next failure mode Alkali-aggregate reaction is a similar process as DEF except in this case alkalis diffuse into the concrete and react with the aggregate in the concrete and cause expansion and cracking leading to complete failure (Thomas Telford 1992). These processes are displayed in figures 2.2 and 2.3.
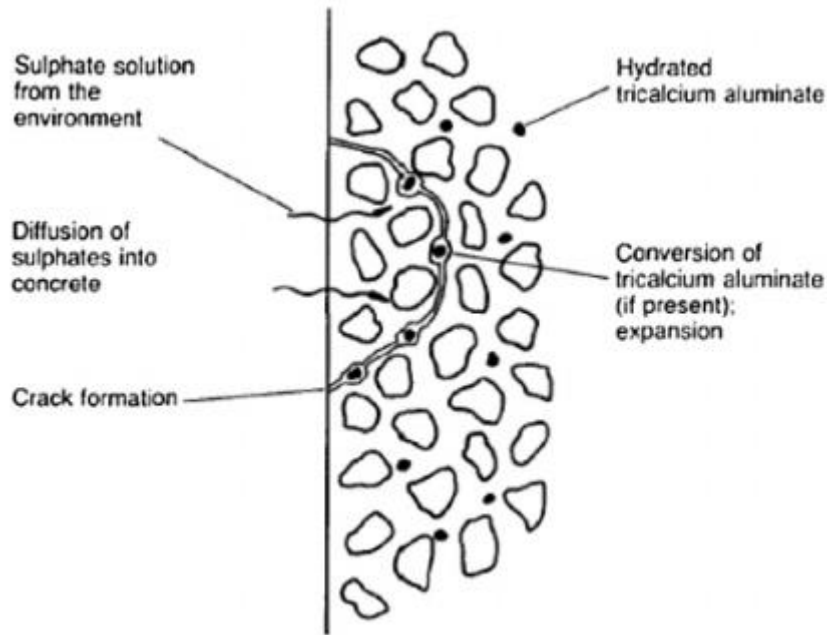
Figure 2.2: Delayed ettringite formation (DEF) process (Ferdous and Manalo 2014).
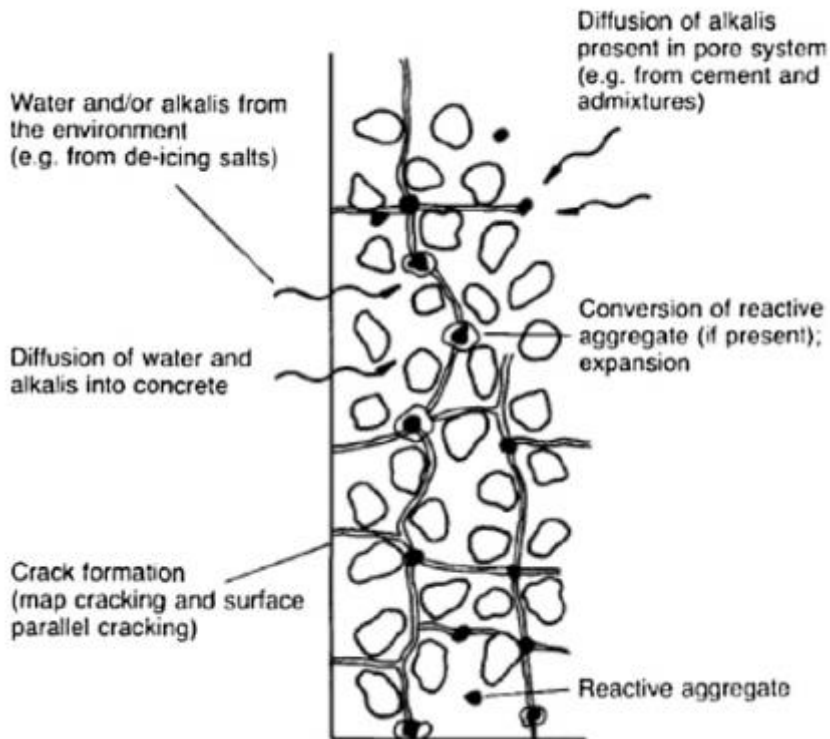
Figure 2.3: Alkali-aggregate reaction (AAR) failure (Ferdous and Manalo 2014).

The next concrete sleeper failure mode is due to acid attack in the concrete. As explained by Ferdous and Manalo (2014) acid rain can be caused by industries and vehicles emitting sulphur dioxide and nitrogen oxide into the atmosphere which can then be spread great

distances due to the wind and end up reacting with the cement in the concrete sleepers which destroys the structural integrity of the material.

Bar corrosion is another serious issue with concrete sleepers that commonly prevents them from reaching their target design life. As sleepers are subjected to changing weather and environmental conditions they are susceptible to penetration by water and chloride ions which can eventually lead to the corrosion of steel bars. Testing performed by Mohammed et al. (2001) determined that cracking of concrete, regardless of the size of the cracks, can cause significant corrosion of the steel bars due to this penetration of chloride ions. This affects the performance of the sleepers in two main ways: corrosion of the bars reduces the cross section area and therefore the ability to resist tensile forces and the rust produced by the corrosion can deteriorate the surrounding concrete (Taherinezhad et al. 2013). This has led to researches trying different techniques such as adding mineral and chemical additives, using reinforcing fibres and new mix designs to increase the durability of concrete, with limited success in the adaptation of these designs (Taherinezhad et al. 2013). This highlights the importance of the research of this paper in assessing the suitability of concrete sleepers reinforced with GFRP bars, as this new design could be a solution to concrete sleeper durability problems.

The last failure mode considered for concrete railway sleepers is due to ice forming in the sleepers. A study by Zi et al (2012) found that for the Kyengbu railway in Korea approximately 1 sleeper along every 300m of track was affected by ice forming. This failure occurs due to water seeping into cracks near the bottom of the sleeper and freezing creating an ice pressure of approximately 40 MPa which then causes further cracking an eventually complete failure of the sleeper.

2.3   GFRP Bar Properties

2.3.1   The general characteristics of FRP Composites

A composite is a material which utilises a combination of two or more different materials to create an end product which has mechanical and chemical properties far greater than the individual materials. Composite materials consist of a resin material called the matrix and a reinforcement fibre material. The properties of the composite material are determined by the mechanical and chemical interaction of the chosen materials. The advantages of composites materials over traditional materials such as steel and timber include:

- Corrosion resistance

- High strength/low weight

- Dimensional stability

- Excellent electrical properties and low moisture absorption

There are many different types of fibres used in composites with each fibre being classified as either a synthetic or natural fibre. The most commonly used synthetic fibres include glass (E-glass most common glass fibre) which is strong and possesses high heat resistance and electrical properties, and carbon which is light weight and has a very high strength and a modulus of elasticity that can match that of steel. Another synthetic fibre regularly used is Aramid which has a high strength and low density and is used in high impact applications. The most commonly used natural fibres include Sisal, Hemp and Flax which are limited in application due to their low strength and susceptibility to moisture and high humidity (Molded Fibre Glass Companies).

For composite materials used for structural applications thermoset resins are used for the matrix material. The most common types of thermoset resins are Polyesters, Vinylesters, Epoxies and Polyurethanes. Polyesters provide low cost, a balance of good mechanical, chemical and electrical properties and have good dimensional stability. Vinylesters possess chemical resistance and strength and properties. While Epoxies are more expensive, they possess excellent adhesion properties, heat resistance capabilities and higher fatigue properties. The last commonly used thermoset resin Polyurethane possesses high toughness and elongation properties and has faster curing times than other resins (Molded Fibre Glass Companies).

2.3.2 The performance of GFRP bars in reinforced concrete structures

The use of GFRP bars as internal reinforcement in concrete structures is gaining popularity due to its corrosion resistant properties, which makes it suitable for reinforcement of concrete structures in corrosive environments where steel reinforcement will not last. The mechanical properties of FRP bars are different from steel bars as they exhibit a higher tensile strength, a lower modulus of elasticity and have an elastic brittle stress- strain relationship (Ashour, 2005). Due to these properties concrete structures reinforced with

11

FRP bars cannot be designed in the same way as steel reinforced members and therefore research has had to be conducted to develop models which can estimate the flexural and shear capacity of these structures.

Work by Tang, Lo and Balendran (2008) investigated the tensile properties of smooth circular GFRP bar, smooth elliptical GFRP bar and compared the results to a mild steel bar. The results of this investigation shown in table 1, highlight the significantly lower modulus of elasticity of the GFRP bars (approximately 25% of mild steel) and the superior tensile strength/ ultimate yield stress of the GFRP bars (approximately 2.5 times mild steel).

Table 2.2: Comparison of tensile properties of GFRP and mild steel bars (Tang, Lo and Balendran, 2008)

Tension properties of GFRP and mild steel reinforcing bars

Rebar types	Cross-sectional area, A_b (mm^2)	Yield stress (N/mm^2)	Ultimate stress (N/mm^2)	Ultimate strain (%)	Elastic modulus (kN/mm^2)
Gsc	50	—	1150	2.45	47.0
Gse	65	—	1210	2.55	47.5
MS	50	340.4	460	0.18[a]	185.0

[a] Strain at yield point.

2.4 Design of Sleepers

There are different practices adopted in the design of railway sleepers from country to country, although they all comprise the same basic four steps. These include calculation of the rail seat load, determination of a dynamic coefficient factor, assuming an appropriate stress distribution pattern and then analysing a model of the sleeper (Sadeghi and Youldashkhan 2005).

2.4.1 Rail Seat Load

As reported by Jeffs and Tew (1991) the rail seat load is dependent on a number of factors. These include:

- The weight of the rail

- Spacing of the sleepers

- The stiffness of the sleeper

- The track modulus per rail

- The rail pad stiffness

- The amount of play between the rail and the sleeper

- The amount of play between the sleeper and the ballast

The influence that the play between the rail and sleeper and the sleeper and ballast has on the rail seat load is dependent on the level of track maintenance.

There are a number of different researchers who have developed methods to calculate the rail seat load. The most commonly used methods as described in Jeffs and TEW (1991) will be highlighted in this section.

The first method for calculating the maximum rail seat load was developed by Talbot (1918-1934) and Clarke (1957) using a beam on elastic foundation model. This method determined the maximum rail seat load by the following equation:

$$q_r = S \cdot k \cdot ym \cdot F_1 \qquad\qquad (2.0)$$

where q_r = predicted rail seat load

S = sleeper spacing

k = track modulus

ym = the maximum rail deflection caused by the interaction of a number of axle loads about a given reference position

F_1 = factor of safety to allow for variations in track support

O'Rourke (1978) found that for 1.8m spacing between axles in the same bogie and 2.3m spacing between adjacent wagon axles the value of $k \cdot ym$ / unit load was a constant 0.56 for any track modulus. This simplified the previous equation to:

$$q_r = 0.56 \cdot S \cdot F_1 \cdot P \qquad\qquad (2.1)$$

Where P = design wheel load (kN) and the remaining parameters are as previously defined.

13

Research was performed by both AREA (1975) and ORE (1969) to further develop this into two new methods for determining the maximum rail seat load. These methods are presented below:

AREA method:

$$q_r \;=\; Df \; x \; P \tag{2.2}$$

where q_r = maximum rail seat load (kN)

P = design wheel load (kN)

Df = distribution factor, expressed as a proportion of the wheel load.

ORE method:

$$q_r \;=\; \bar{\varepsilon} \cdot c_1 \cdot P \tag{2.3}$$

where P = design wheel load based on ORE formula

$\bar{\varepsilon}$ = dynamic mean value of the ratio $\bar{q}_r / \bar{P}_S$ where $\bar{q}_r$ and $\bar{P}_S$ are the mean values of the rail seat load and static axle load respectively and:

$$c_1 = \varepsilon / \bar{\varepsilon} \tag{2.4}$$

where ε = the maximum value of the ratio q_r / P_S and c_1 is equal to 1.35

The last method considered is the three adjacent sleepers method. This method assumes that as the load moves along the rail it is distributed along three adjacent sleepers with the maximum load considered for one of the sleepers as 50 percent. This formula is shown below:

$$q_r \;=\; 0.5P \tag{2.5}$$

where P = design wheel load

q_r = predicted maximum rail seat load.

The Australian Standard for Prestressed sleepers AS1085.14 (2012) follows a similar method for determining the rail seat load as the AREA method. The difference being that the Australian standard method determines the vertical design wheel load incorporating a dynamic coefficient first and then applies the distribution factor. The method can be seen below:

$$P_{dV} = k_s Q \qquad\qquad (2.6)$$

Where k_s = dynamic coefficient, default value of 2.5 when no field measurements are available.

Q = maximum static wheel load (kN)

P_{dV} = vertical design wheel load (kN)

$$R_V = P_{dV} DF / 100 \qquad\qquad (2.7)$$

Where DF = load distribution factor from figure 3.1 of AS1085.14 (figure 1.3)

P_{dV} = vertical design wheel load (kN)

R_V = vertical design rail seat load (kN)
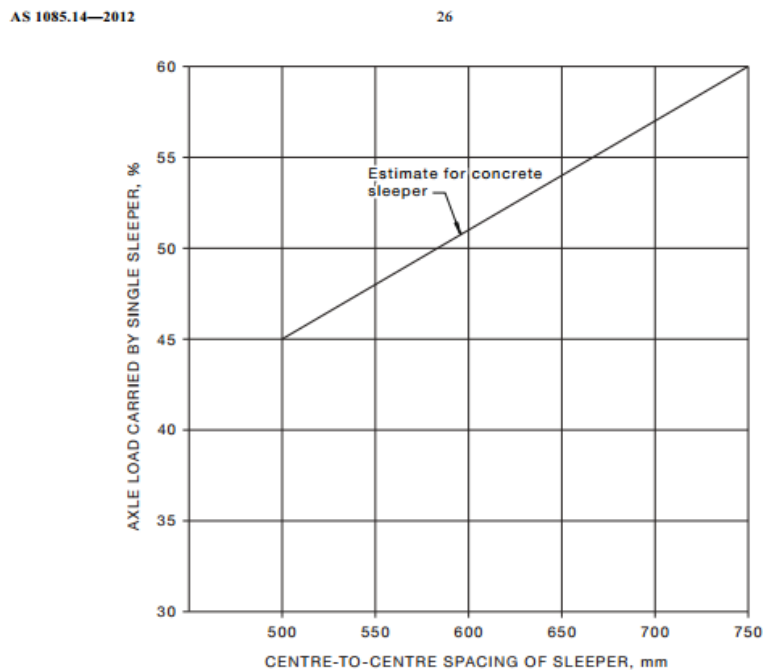
Figure 2.4: Axle Load Distribution Factor (AS1085.14, 2012)   It is interesting to note that figure 2.3 adopts the Distribution Factor line for concrete sleepers proposed by AREA (1985).

2.4.2   Dynamic Coefficient Factor

In the design of railway sleepers, the rail loads are considered as static. Due to the movement of the train the loads experienced by the sleepers can be much higher than that of just the dead load of the train. To account for this a dynamic coefficient factor is applied to the static rail load. A review of the related literature by Sadeghi and Youldashkhan (2005) revealed that there are many different methods to calculate an appropriate dynamic coefficient factor. These methods have been summarised in table 2.3. Where V is the velocity of the train in km/hr, D is the diameter of the wheel in mm, K is the modulus of the rail support in MPa, g is the gauge width in mm, α' and β' are in relation to the mean value of impact factor and γ' is related to the standard deviation of the impact factor, P_u is unsprung weight of one wheel, D_j is the track stiffness at the joints in kN/mm and $(\alpha_1 + \alpha_2)$ is the total rail joint dip angle in radians.

Table 2.3: Relationships for dynamic coefficient factors. (Sadeghi and Youldashkhan 2005).

Standard	Relation
AREA[17]	$\Phi = 1 + 5.21\dfrac{V}{D}$
Eisenmann [18]	$\Phi = 1 + \delta\eta \ t$
ORE [16]	$\Phi = 1 + \alpha' + \beta' + \gamma'$
DB [20]	$\phi = 1 + \dfrac{V^2}{30000}$, $\phi = 1 + \dfrac{4.5\,V^2}{10^5} - \dfrac{105\,V^3}{10^7}$
BR [21]	$\Phi = \dfrac{8.784(\alpha_1 + \alpha_2)\,V}{P_s}\left[\dfrac{D_j\,P_u}{g}\right]^{1/2}$
India [22]	$\phi = 1 + \dfrac{V}{58.14\,k^{0.5}}$
South Africa[23]	$\phi = 1 + 4.92\dfrac{V}{D}$
CA [24]	$\phi = 1 + \dfrac{19.65\,V}{D\,K^{1/2}}$
WMMTA [24]	$\phi = (1 + 3086 * 10^{-5}\,V^2)^{0.67}$
SADEGHI [25]	$\phi = 1.098 + 8 \times 10^{-4}\,V + 10^{-6}\,V^2$

2.4.3 Bearing Pressure Patterns

The sleeper support condition and the coinciding contact pressure distribution between the sleeper and the ballast must be determined before the structural behaviour of the sleeper under the train loading can be calculated. The degree of voiding of the ballast below the sleeper controls the pressure distribution and as voiding occurs gradually under the repeated train loading, the pressure distribution will vary over time depending on the level of maintenance (Jeffs and Tew, 1991).

ORE (1969) concluded that it is practically impossible to determine the exact pressure distribution for an in service sleeper. Therefore, a number of hypothetical pressure distribution patterns have been developed, according to different levels of ballast condition, to allow efficient structural design of sleepers. The hypothetical bearing pressure distributions currently considered in practice are displayed in table 2.4.

To accurately analyse pattern two of table 2.4 the effective length of the sleeper support at the rail seat must be determined. Sadeghi and Youldashkhan (2005) have summarised the main methods currently used in practice to determine the effective sleeper support length. This can be seen in table 2.5.

Table 2.4: Hypothetical sleeper bearing pressure distributions (Sadeghi and Youldashkhan 2005).
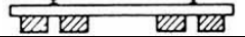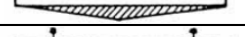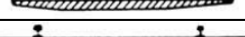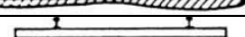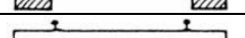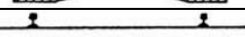
Item No.	Distribution of bearing pressure	Developers	Remarks
1		ORE[16],Talbot[7]	Laboratory test
2		ORE[6],Talbot[8],Battelle[9],Clarke[10]	Tamped either side of rail
3		ORE[19],Talbot[8]	Principal bearing on rails
4		ORE[19],Talbot [8]	Maximum intensity at ends
5		Talbot[8]	Maximum intensity in middle
6		Talbot[7]	Center bound
7		Talbot[7]	Flexure of sleeper produces variations form
8		ORE[19],Talbot[8],kerr[11],Schramm[12]	Well tamped sides
9		ORE[19],Talbot[8]	Stabilized rail seat and sides
10		AREA[13],Raymond[14],Talbot[8]	Uniform pressure

Suggestion by:	Effective Length of sleeper support at the rail seat
AREA[13]	Distance from the end of the sleeper to the point inside of the edge of the rail base over which tamping operations extend
Clarke[10]	$L = (l-g)\left(1 - \dfrac{(l-g)}{125t^{0.75}}\right)$ in which l, g, and t are total sleeper length (mm), distance between the center-line of rail seats (mm), and sleeper thickness (mm), respectively.
Schramm[12]	$L = \dfrac{l-g}{2}$
Simplified Clarke[10]	$L = \dfrac{l}{3}$

2.5   Analytical Solution

An analytical solution to the problem of a sleeper analysed as a beam on an elastic foundation has been derived by Hetenyi (1967) to calclate the bending moment at the rail seat, sleeper centre and the maximum deflection at the rail seat region. A diagram of the problem analysed can be seen in figure 2.6. The analysis considers the two vertical rail loads and a uniform bearing pressure distribution. The derived bending moment and deflection equations are also presented below.
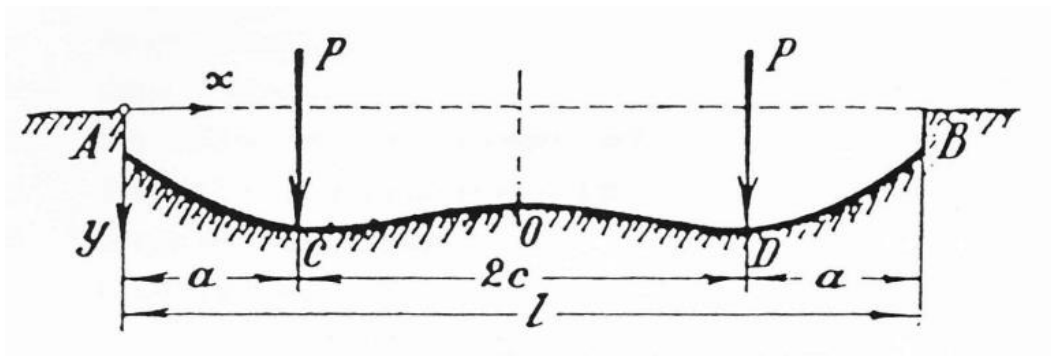
Figure 2.5: A schematic of the sleeper analysed as a beam on elastic foundation (Jeffs and Tew 1991).

$$M_{A-C} = \frac{RSL}{2\lambda} \frac{1}{\sinh \lambda \iota + \sin \lambda \iota} \Big\{ 2 \sinh \lambda x \sin \lambda x \big[\cosh \lambda a \cos \lambda (\iota - a)$$
$$+ \cosh \lambda (\iota - a) \cos \lambda a \big] + (\cosh \lambda x \sin \lambda x$$
$$- \sinh \lambda x \cos \lambda x) \big[\cosh \lambda a \sin \lambda (\iota - a) - \sinh \lambda a \cos \lambda (\iota - a)$$
$$+ \cosh \lambda (\iota - a) \sin \lambda a - \sinh \lambda (\iota - a) \cos \lambda a \big] \Big\}.$$

Figure 2.6: Moment in the region A-C (Jeffs and Tew 1991).

$$M_o = -\frac{RSL}{2\lambda} \frac{1}{\sinh \lambda \iota + \sin \lambda \iota} \Big\{ \sinh \lambda c \big[\sin \lambda c + \sin \lambda (\iota - c) \big]$$
$$+ \sin \lambda c \big[\sinh \lambda c + \sinh \lambda (\iota - c) \big]$$
$$+ \cosh \lambda c \cos \lambda (\iota - c) - \cos \lambda c \cosh \lambda (\iota - c) \Big\}$$

Figure 2.7: Moment at the sleeper centre (Jeffs and Tew 1991).

$$y_{max} = \frac{RSL.\lambda}{K_s} \frac{1}{\sinh \lambda \iota + \lambda \iota} \Big\{ \cosh \lambda c \big[\cos \lambda (\iota - c) + \cos \lambda c \big]$$
$$+ \cos \lambda c \big[\cosh \lambda (\iota - c) + \cosh \lambda c \big]$$
$$- \sinh \lambda c \sin \lambda (\iota - c) + \sin \lambda c \sinh \lambda (1 - c) \Big\}$$

Figure 2.8: Maximum deflection of sleeper (Jeffs and Tew, 1991).

Where M_{A-C} = moment in the region A – C

M_O = moment at sleeper centre

l = sleeper length

RSL = design rail seat load

X = distance from end of sleeper

c = distance from rail seat load to sleeper centre

a = distance from sleeper end to rail seat load

λ = sleeper stiffness parameter = $(K_S/4. E_S.I_S)^{0.25}$

K_S = sleeper support modulus (N/m^2)

E_S = Young's modulus of sleeper (N/m^2)

I_S = sleeper moment of inertia about horizontal neutral axis (m^4)

y_{max} = deflection at the rail seat region (m)

2.6   2.6 Summary of research in the area

This section provides a summary of some of the previous work on the design of railway sleepers and also research on the application of GFRP in railway sleepers. As a part of this research the bearing distribution patterns highlighted in previous sections will be analysed to determine which one gives the highest design forces and therefore allow the ultimate strength design of the sleeper. Figure 2.10 highlights the typical bending moment diagram shape for the different bearing pressure distributions, as developed by Jeffs and Tew (1991). These will be useful when assessing the accuracy of the flexural results in chapter 3.
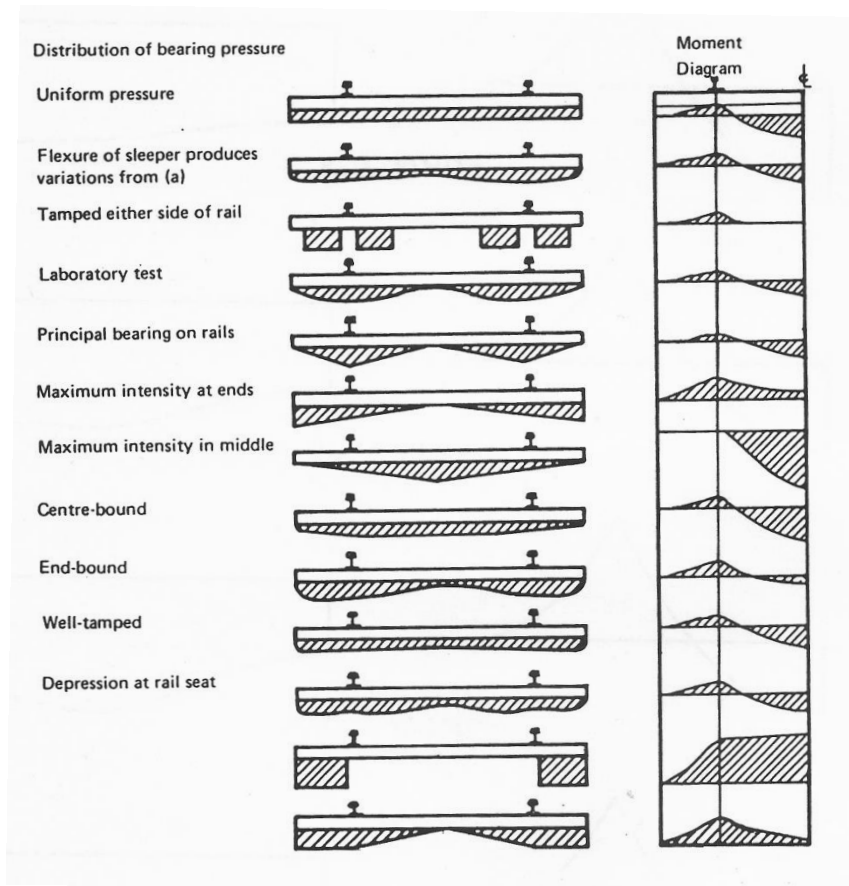
Figure 2.9: Proposed distribution of sleeper bearing pressure and bending moment diagrams (Jeffs and Tew, 1981).

Research similar to the parametric study that will be conducted as a part of this research has been performed by Manalo et.al (2012). This paper considers a simplified grillage beam analogy to investigate the behaviour of a railway turnout sleeper with varying elastic modulus and support modulus values. The aim of the study was to determine suitable parameters for a new fibre composite sleeper design. This research found that the change in support modulus and in particular the sleeper modulus has a considerable effect on the maximum bending moment experienced by the sleepers. The change in support modulus from 10 to 40 MPa resulted in a 15% increase in the maximum bending moment while the change in sleeper modulus from 1 to 10 GPa resulted in a significant increase of up to 75% in bending moment. The resulting effect of changing the support and sleeper modulus on the bending moment, deflection and pressure experienced by the sleeper, can be seen in figures 2.11 and 2.12.
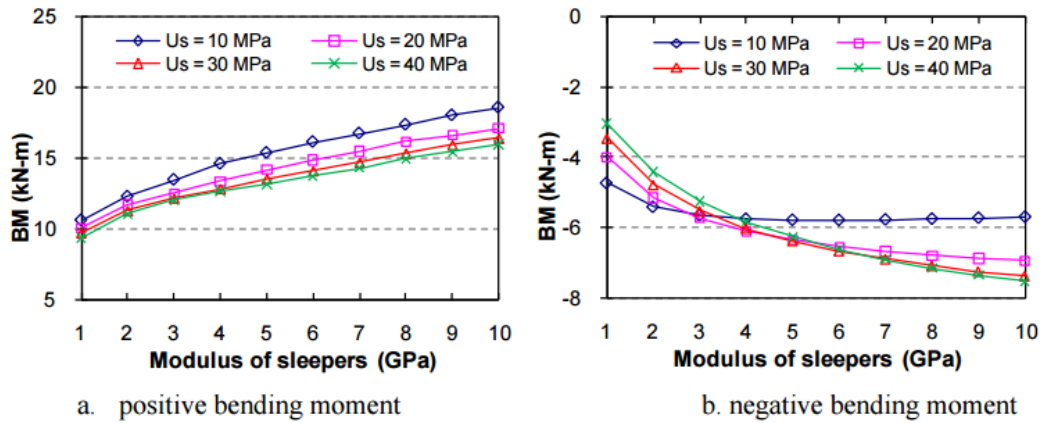
Figure 2.10: Maximum bending moment for varying parameters (Manalo et.al, 2012).
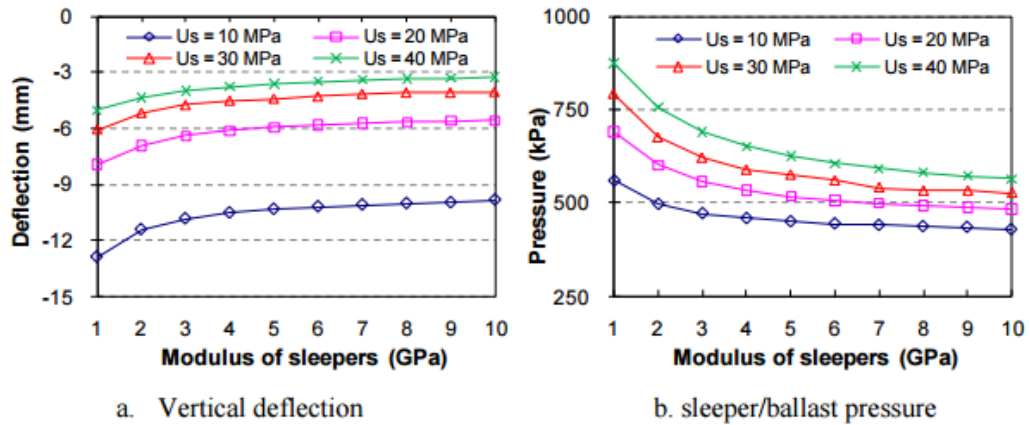
Figure 2.11: Vertical deflection and sleeper ballast pressure for varying parameters (Manalo et.al, 2012).

The key findings of this study were that the shear forces in the turnout sleepers were not sensitive to changes in these parameters, a sleeper modulus of 4 GPa was found to be optimal for the new fibre composite sleeper as long as a support modulus of 20 MPa or greater was maintained for the ballast. This study will be a valuable reference for comparing the results of the parametric study later in this dissertation.
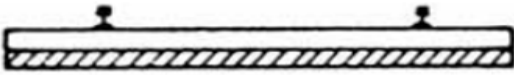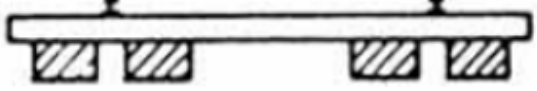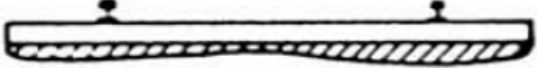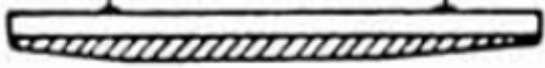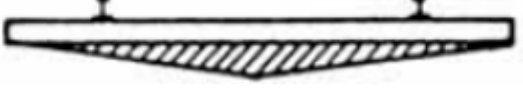
CHAPTER 3 Design and Analysis of Sleepers

3.1 Stage 1 Overview

Stage 1 involves analysing a concrete sleeper for each of the bearing pressure distributions from the available literature, as displayed in table 3.1. For this stage of the analysis the 10 patterns will be considered, with each pattern analysed for 4 typical support modulus values, 10 MPa, 20 MPa, 30MPa and 40 MPa (Jeffs and Tews 1991). The design bending moments, shear force and deflection for each pattern will be recorded and compared to the corresponding values calculated from AS1085.14 and the beam on elastic foundation method where available.

The results from this stage will determine the bearing pressure patterns which give the highest design bending moments (both positive and negative) and shear forces. This will provide the bending moment and shear force envelope for which the required top and bottom tensile reinforcement and shear reinforcement (if any is required) can be designed throughout the length of the sleeper. The identified critical patterns can then be adapted for stage 2, where parametric studies will be performed to determine the combination of sleeper parameters which produce the highest design forces. From this the final GFRP reinforced sleeper design can be chosen and its performance compared to a traditional steel reinforced concrete sleeper.

Table 3.1: Bearing pressure distribution patterns adopted for analysis.

No.	Bearing Pressure Distribution Pattern
1	
2	
3	
4	
5	
6	
7	
8	
9	
10	

3.2   Developing the model

3.2.1   Rail Parameters and Load

The first step of completing stage 2 was to define rail parameters and calculate the rail load. For this project a Queensland railway sleeper is being considered so the rail gauge g is taken as 1067mm with the distance between rail centres G = 1137mm. A 25 tonne design axle load was considered for this first stage of the project analysis (Manalo et al. 2012). With these parameters defined the method for determining the rail seat load provided in AS1085.14 (2012) was then followed.

Calculation of the vertical design wheel load using equation 2.6:

$$P_{dV} = k_s Q$$

Where Q = 25tonnes/2 wheels = (25/2) tonnes x 9.81m/s^2 = 122.63 kN, and

k_s is assumed as 2.5 due to the lack of field measurements.

$$P_{dV} = 2.5 \text{ x } 122.63 \text{ kN} = 306.58 \text{ kN}$$

Calculation of the vertical design rail seat load:

$$R_V = P_{dV} DF / 100$$

Where DF = load distribution factor from figure 3.1 of AS1085.14

Adopting a sleeper spacing of 600mm gives a *DF* value of 52% from figure 1.3.

$$R_V = 306.58 \text{ kN x } (52/100) = 159.42 \text{ kN}$$

Therefore, the approximate vertical rail load that will be assumed for the analysis is 160 kN.

3.2.2   Concrete sleeper model parameters

Before the model can be created the properties and dimensions of the concrete sleeper must be quantified. For this first stage of the analysis typical concrete properties were assumed and a typical narrow gauge concrete sleeper size was adopted and simplified to a constant rectangular section. The details of the concrete sleeper parameters can be seen in table 3.2.

The rail base width was also needed for modelling some of the patterns. A typical value of 146mm for a 60kg/m rail was used (AS1085.1, 2012). The effective length of sleeper

support at the rail seat was also required to correctly analyse bearing distribution 2. The simplified Clarke method (Table 2.5) was used to calculate a length of 0.717m.

Table 3.2: Properties of the sleeper model.

Item	Value
Sleeper length	2.15m
Sleeper height	0.25m
Sleeper width	0.18m
Concrete Density	2500 kg/m^2
Young's Modulus	30 GPa
Poisson's Ratio	0.15
Rail base width	0.146mm

3.2.3   Finite Element Model

With all the required parameters now chosen the sleeper was then modelled using the Finite Element Software Strand7. A 3dimensional view of the concrete sleeper model can be seen in figure 3.1.
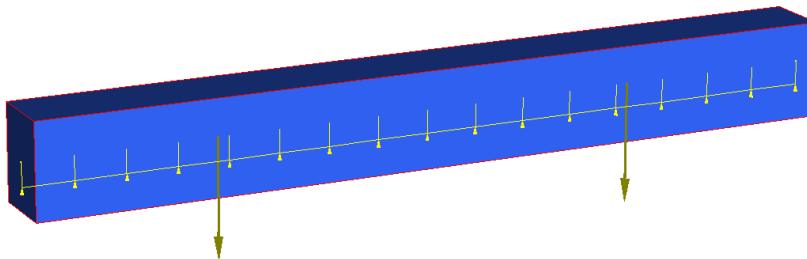
Figure 3.1: 3-D view of the concrete sleeper model.

Due to the differences in the patterns some of the elements had to be subdivided at different positions. Most noticeably pattern 2 and 3 had to be subdivided so that the pattern could be correctly modelled allowing for the rail width. Pattern 1 was simply modelled as one element due to the constant bearing pressure.

The remaining cases which had linear or parabolic variations in the support modulus along the length of the beam were more complex due to fact that the elastic support function in Strand7 only allows a constant support modulus for each element. To overcome this the sleeper model was subdivided into 20 elements (5 equal sections for the end portions and 10 equal sections for the middle portion). The subdivision for the various patterns is illustrated in figures 3.2 – 3.5.

Figure 3.2: Subdivision of the model for pattern 3.

Figure 3.3: Subdivision of the model for pattern 2.
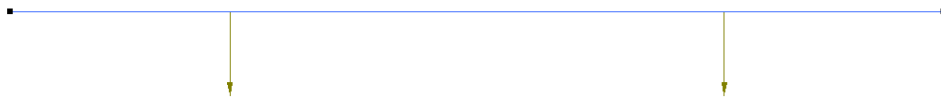
Figure 3.4: Subdivision of the model for pattern 1.
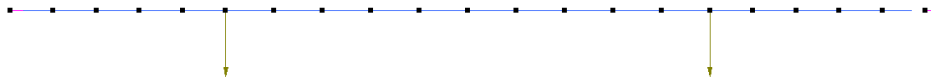
Figure 3.5: Subdivision of the model for pattern 4, 5, 6, 7, 8, 9 and 10.

The variation of the support modulus distribution along the beam was approximated by taking average modulus values for the individual sections and assigning those values to each section. The analysis was then performed and the bending moment, shear force and deflection data for each typical modulus value were graphed. The bending moment results are also compared to the design values suggested in AS1085.14 and the model is verified against the analytical solution for pattern 1.

3.3   Strand7 Model Verification

It is critical that the results of the strand7 model are verified using the analytical solution of a sleeper analysed as a beam on elastic foundation, to ensure the model produces accurate results and therefore gives the work credibility. To verify the model, the results from pattern 1 (Table 3.1) for the bending moment and deflection were compared to the corresponding values obtained for the same pattern using the beam on elastic foundation solution as presented in section 2.5.

From tables 3.3 and 3.4 it can be seen that the results of the Strand7 model almost exactly match the results from the analytical solution for the bending moments. This comparison also highlights that there is an approximately 20 – 30% variation in calculated deflection values between the two analysis methods. Although there is a difference in the deflection results, this comparison was considered as sufficient to verify the model as the major performance criteria that is considered for designing sleepers is bending stress, which the strand7 model accurately predicts.

Table 3.3: Results of Analytical solution for pattern 1.

Analytical Results				
U_S (Mpa)	10	20	30	40
M_{A-C} (kN.m)	18.945	18.811	18.689	18.577
M_O (kN.m)	-5.188	-5.388	-5.566	-5.725
y_{max} (mm)	12.558	6.042	3.950	2.931

Table 3.4: Results of Strand7 model for pattern 1.

Strand7 Results				
U_S (Mpa)	10	20	30	40
M_{A-C} (kN.m)	18.944	18.811	18.689	18.577
M_O (kN.m)	-5.188	-5.388	-5.566	-5.725
y_{max} (mm)	14.95	7.504	5.023	3.783

3.4   Results and Discussion

The aim of this stage of the analysis is to evaluate and compare the proposed theoretical bearing pressure distribution patterns for calculating the bending moment and shear forces that sleepers are subjected to and determine which pattern will give the most conservative design forces, for stage 2 of the analysis. To achieve this comparison, the results from the strand7 model for bending moment, shear force and deflection are graphed for the 10 patterns for the varying support modulus values.

3.4.1   Positive and Negative Design Bending Moment

The bending moments recorded for the 10 patterns for each of the support modulus values can be seen graphed below in figures 3.6 – 3.9.
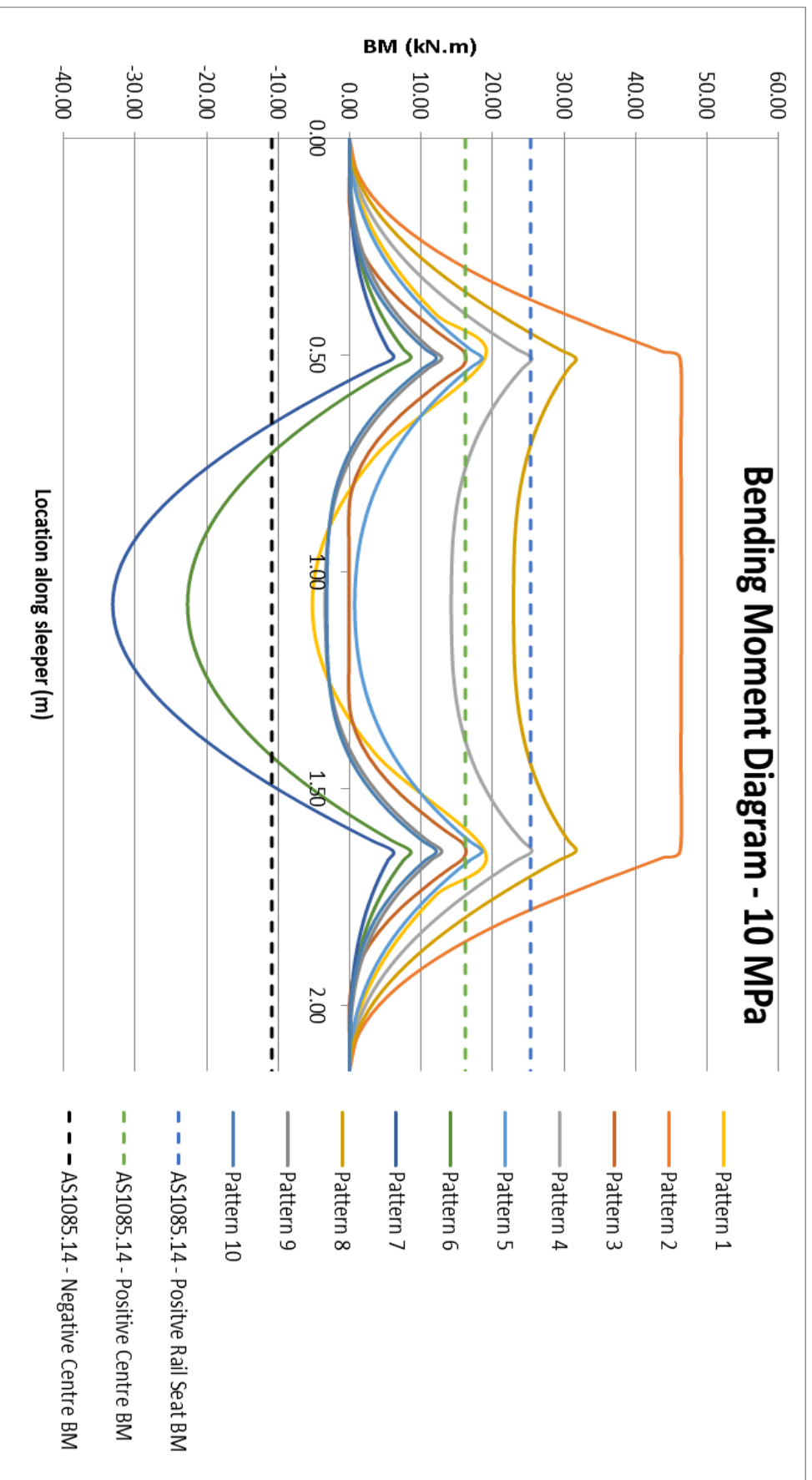
Figure 3.6: Bending Moment Diagram Us 10 MPa.
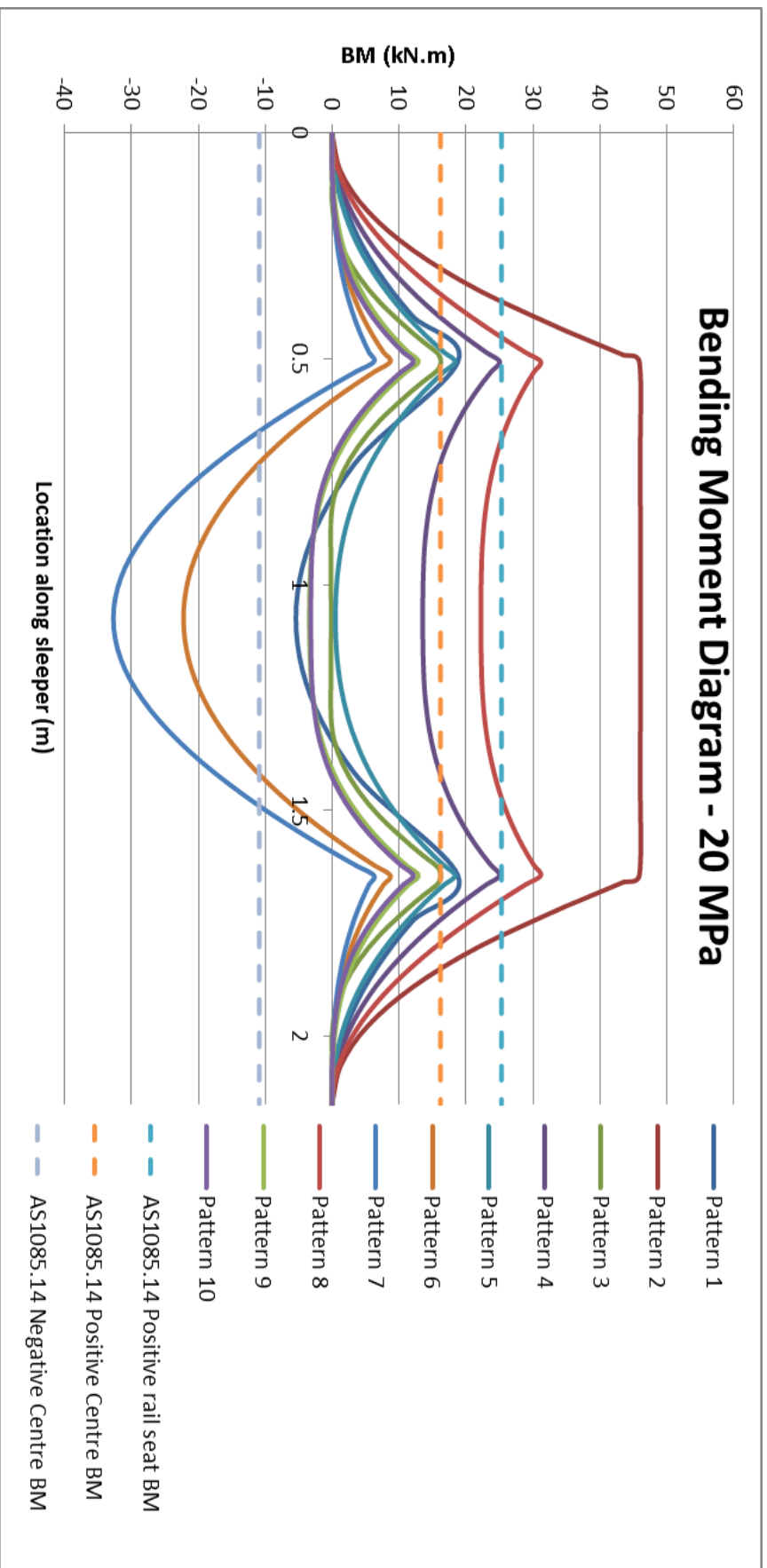
Figure 3.7: Bending Moment Diagram Us 20 MPa.
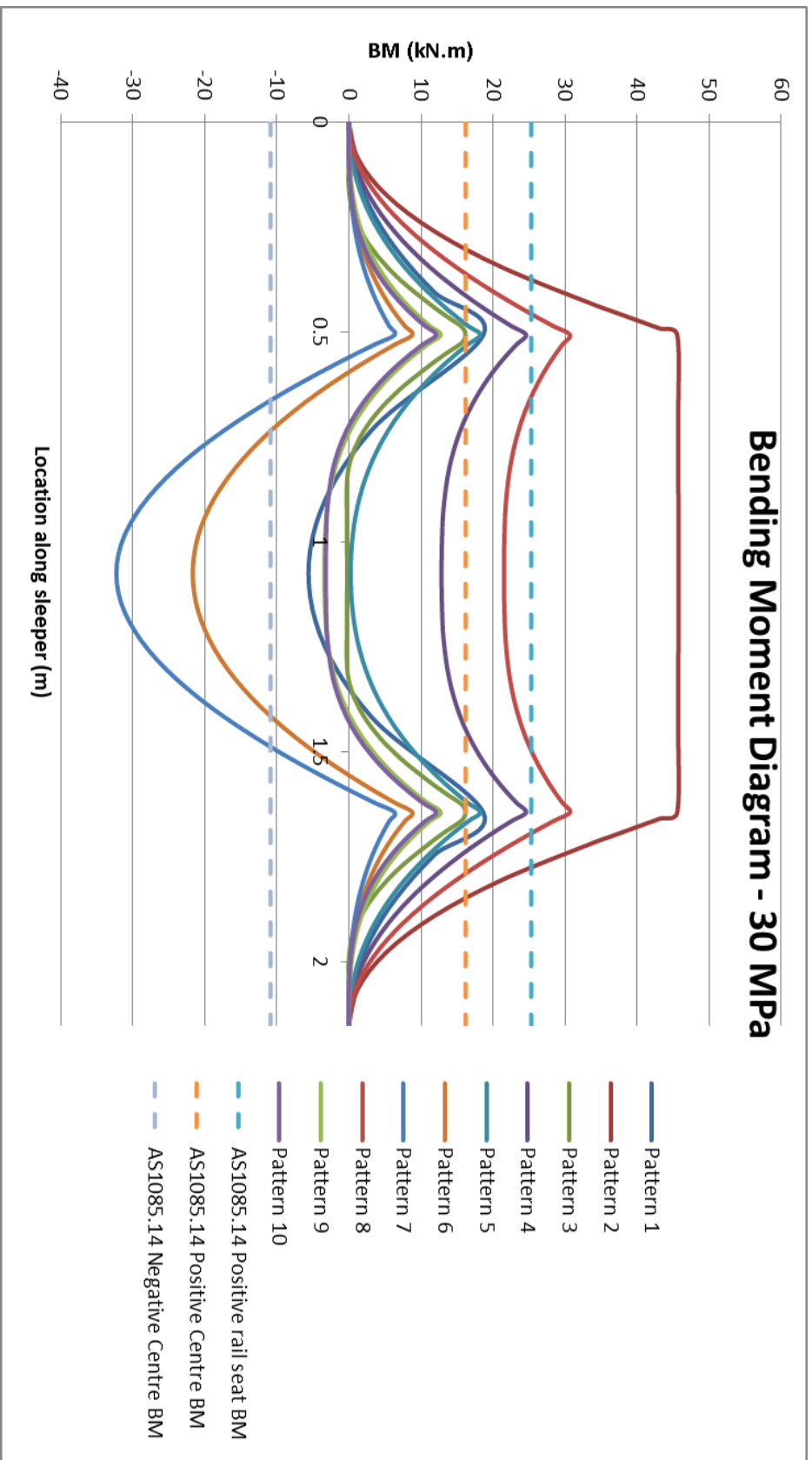
Figure 3.8: Bending Moment Diagram Us 30 MPa.
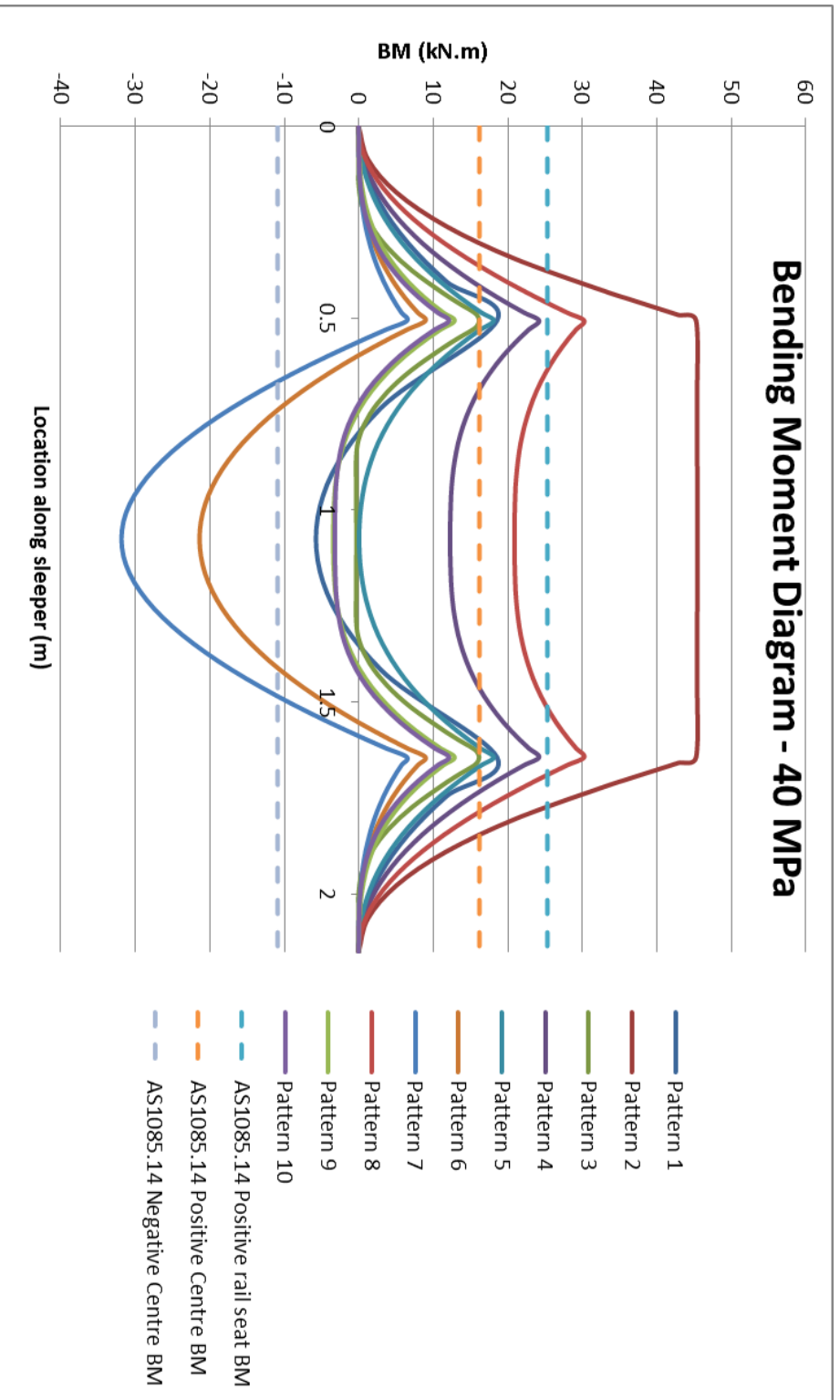
Figure 3.9. Bending Moment Diagram Us 40 MPa.

33

From these graphs it can be seen that pattern 2 experiences the highest bending moment at both the rail seat location and the sleeper centre, with values of approximately 46.2 – 45.3 kN.m and 46.4 – 45.5 kN.m respectively in the order of increasing support modulus. The high positive bending moment at the rail seat and sleeper centre is expected as this pattern represents the ballast condition where the side ballast has been well compacted and there is gaping of the ballast under the centre. This means the rail load is supported by only a small section of ballast at the side; therefore, there is no resistance to bending at the centre of the sleeper.

Following this pattern 4 and 8 have quite a similar bending moment diagram, with their rail seat moments varying from 25.5 – 24.2 kN.m and 31.7 – 30.3 kN.m respectively, while their centre bending moments vary from 14.2 – 12.3 kN.m and 22.9 – 20.9 kN.m respectively. Patterns 1,3,5,9 and 10 bending moments all follow a similar shape with smaller rail seat moments and close to zero bending moment at the centre. The bending moments at the rail seat for this group vary from 6.13 – 18.5 kN.m for 10 MPa modulus and 5.77 – 18.6 kN.m for 40 MPa modulus, while the centre bending moments exhibit a similar range with values of 0.733 to – 4.22 kN.m and 0.07 to – 4.76 kN.m for support modulus 10 MPa and 40 MPa respectively. The last two patterns, 6 and 7 are both of a very similar shape with a very low bending moment at the rail seat but a large negative bending moment at the centre. The values for pattern 6 and 7 at the rail seat vary from approximately 7.59 – 8.98 kN.m and 6.13 kN.m respectively, while at the centre vary from -22.6 to – 21.4 kN.m and -33.1 to -31.8 kN.m respectively.

This visual representation of the bending moment results also allows an interpretation of what support conditions are assumed for the calculation of design bending moments in AS1085.14 Prestressed concrete sleepers. From figures 3.6 – 3.9, the closest fit for the design positive rail seat bending moment and the design positive centre bending moment is pattern 4 with values of 25.51 and 14.23 kN.m with 10 MPa support, compared to the standard values of 25.325 and 16.21 kN.m. From this it can be deduced that for the positive design moments a pattern similar to pattern 4 must have been considered with constant bearing pressure between the ends and the rail and then decreasing pressure from the rail to the centre of the sleeper. This pattern seems to be a reasonable assumption for the design positive bending moments as this deteriorated ballast condition is more likely to occur in practice than pattern 2.

The standard value for the design negative centre bending moment is greater than 10.86 kN.m so this means that only patterns 6 and 7 meet this requirement. While for the negative bending moment a distribution similar to pattern 6 or 7 must have been assumed with

increasing pressure towards the centre of the sleeper. These patterns both have high stress concentrations at the centre of the sleeper as there is higher bearing resistance at this location. This creates negative curvature of the sleeper centre and therefore high negative bending moments. This type of pattern seems like an accurate prediction for negative bending as the ballast could be deteriorated from the outside in due to a combination of cyclic loading at the rail seat and environmental conditions.

The bending moment diagrams developed in strand 7 match quite closely the expected bending moments from the published literature (figure 2.10). In comparison of figure 2.10 and the recorded results, it is concluded that the strand7 results are reasonable. In particular the critical patterns 2 and 7 match the expected bending moment diagram shape quite closely. Pattern 2 increases sharply from the end of the sleeper until the rail load, and then is practically flat from the rail to the sleeper centre, which matches the literature. The calculated bending moment diagram for Pattern 7 is also very similar to the expected result from the literature. In comparing figure 3.6 to figure 2.10, it is seen that the shape from the rail to the centre of the sleeper is approximately the same, although there is a small positive bending moment at the rail seat from the calculated results compared to no bending from the rail to the end of the sleeper for the proposed bending moment diagram. This slight difference could be due to different support modulus and/or rail seat loads. Furthermore, based on these comparisons both the critical patterns appear to be accurate and will be considered for determining the maximum bending moments for the sleeper design.

3.4.2 Shear forces

The shear force diagrams from the strand7 model can be seen in figures 3.10 – 3.13. From these figures it is clear that pattern 2 gives the highest design shear forces acting on the sleeper. The point of maximum shear occurs to the left of the rail with the value remaining at approximately 160.7 kN for all support modulus values. This is quite high compared to pattern 7 which has the next highest shear force, which ranges from approximately 120 to 115 kN for increasing support modulus. It can also be seen that besides pattern 1 and 2 the rest of the bearing pressure distribution patterns give a similar shear force diagram shape.

The reason for such a large shear force occurring for pattern 2 is because the ballast only provides resistance to the rail load for a small section of the sleeper compared to the other patterns. Further to this pattern 7 also experiences a high shear force at the rail seat as the majority of the bearing resistance occurs at the centre of the sleeper. The remaining patterns result in similar shear force diagrams as the stresses induced by the rail load are more

evenly distributed. From these results it is clear that pattern 2 should also be chosen for the calculation of design shear forces for the final sleeper design.
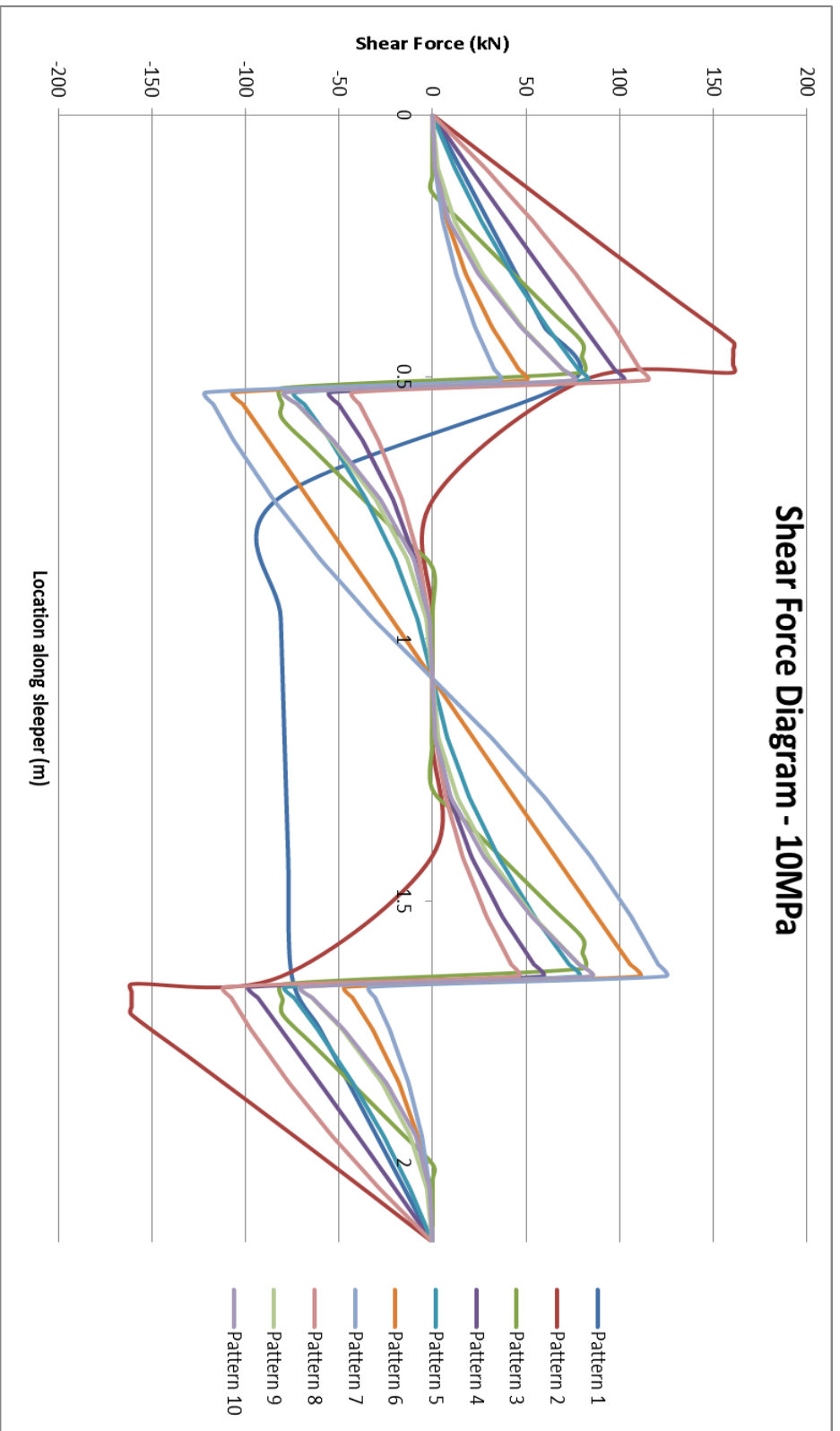
Figure 3.10: Shear Force Diagram Us 10 Mpa
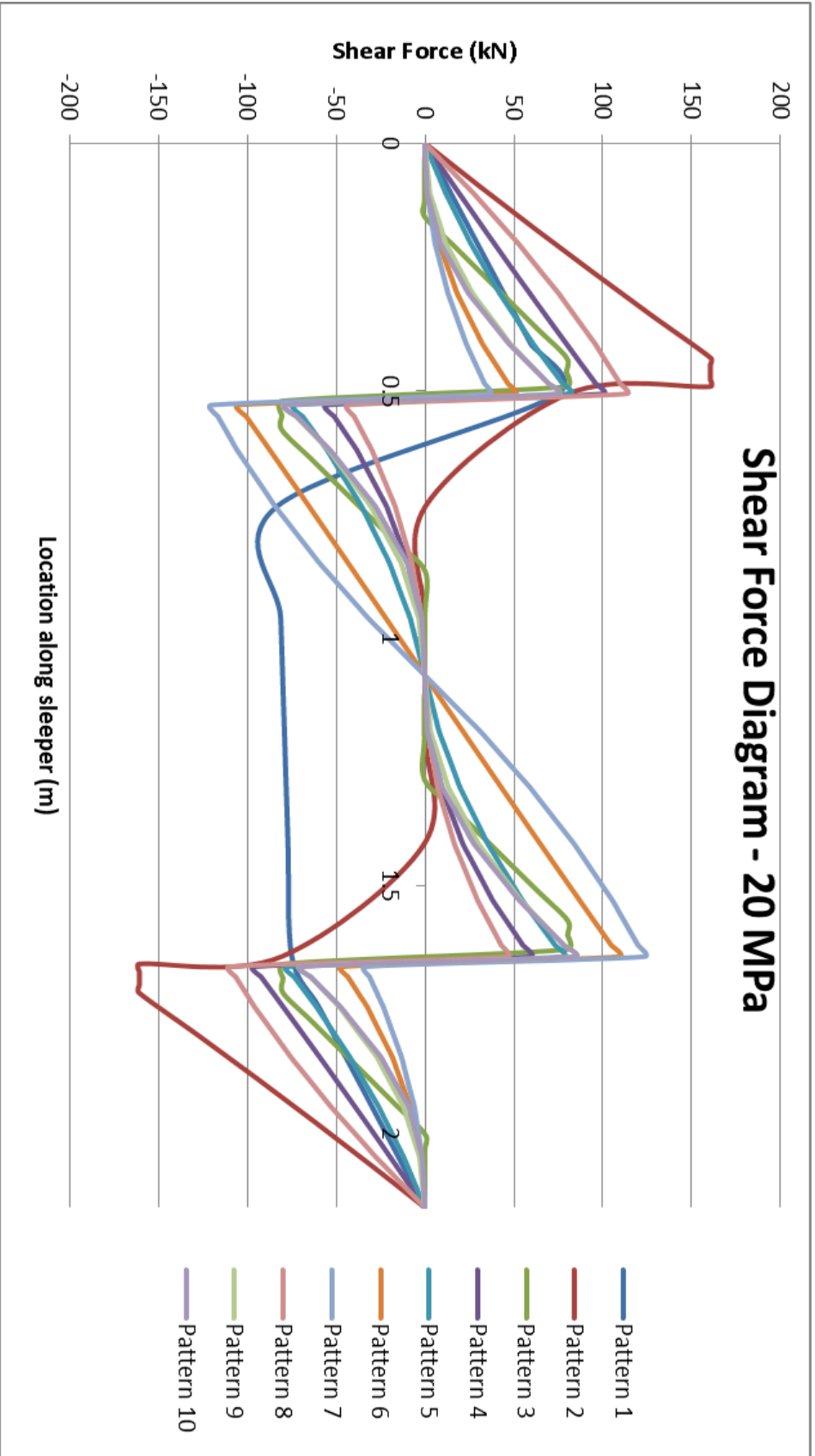
Figure 3.11: Shear Force Diagram Us 20 MPa.
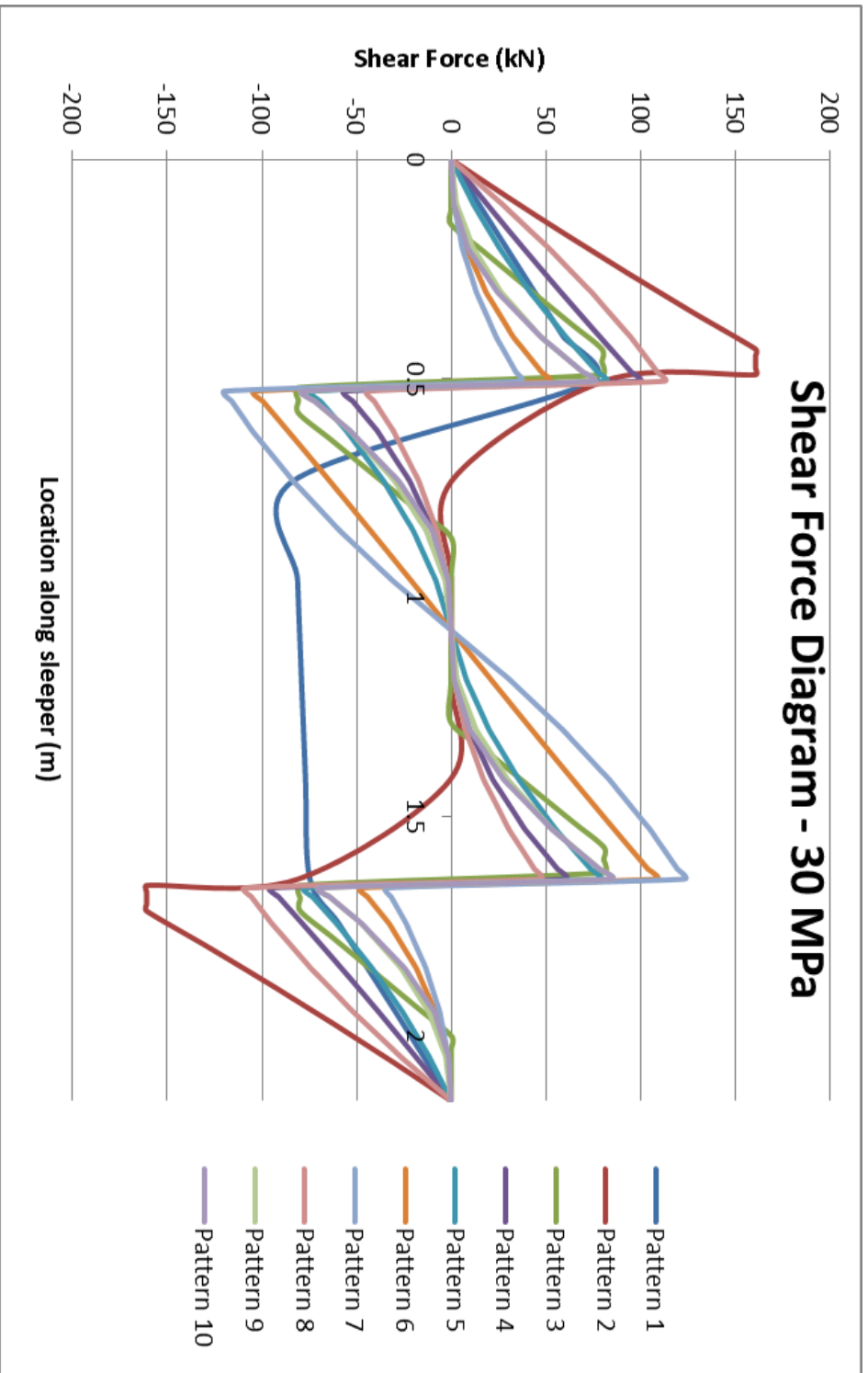
Figure 3.12: Shear Force Diagram Us 30 MPa.

39
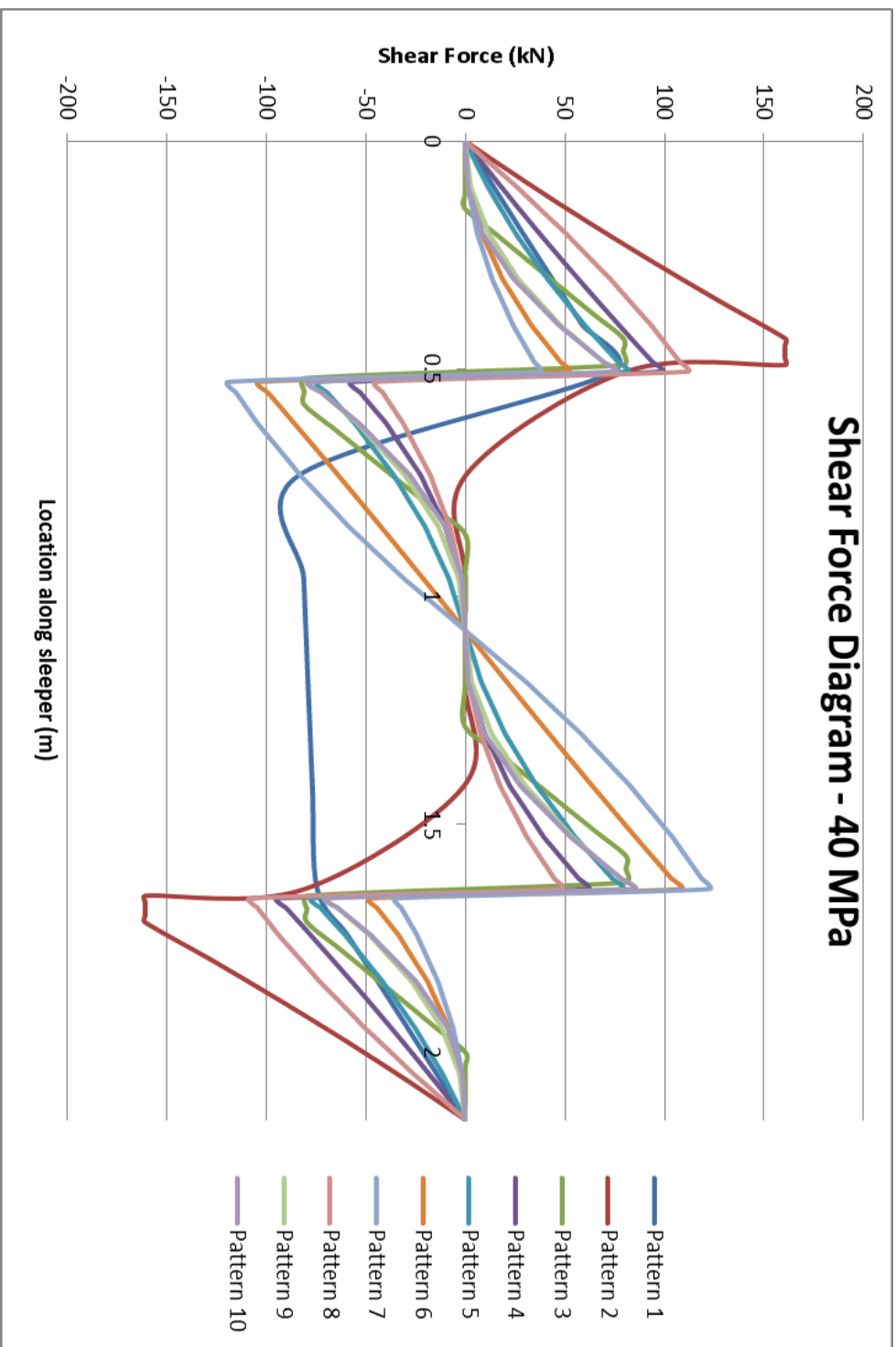
Figure 3.13: Shear Force Diagram Us 40 MPa.

3.4.3 Deflection

The deflection data from the strand 7 analysis for support modulus values 10 MPa, 20 MPa, 30 MPa and 40 MPa can be seen in figures 3.14 – 3.17. From these figures it can be seen that pattern 2 subjects the sleeper to the most deflection. This is expected as pattern 2 also produces the largest bending moment and shear forces. The graphs also highlight that patterns 1, 3, 5, 9 and 10 produce almost no variation in deflection along the length of the sleeper, while for pattern 2, 4 and 8 deflection increases towards the centre and for patterns 6 and 7 the opposite occurs with increasing deflection towards the ends of the sleeper. The results of this analysis suggest that the deflection of the sleepers will be largely dependent on what support modulus value is chosen.
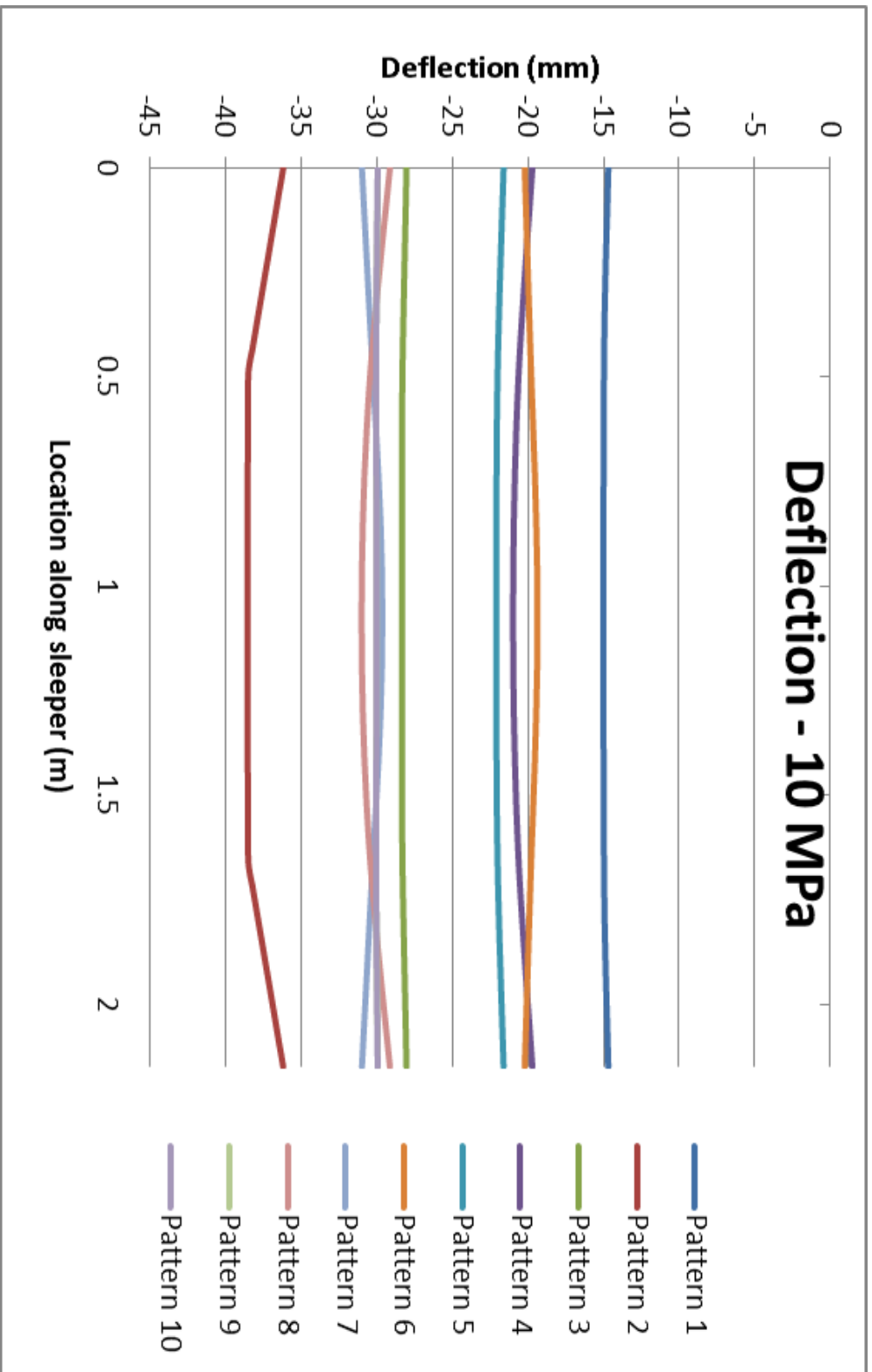
Figure 3.14: Deflection Us 10 MPa

42
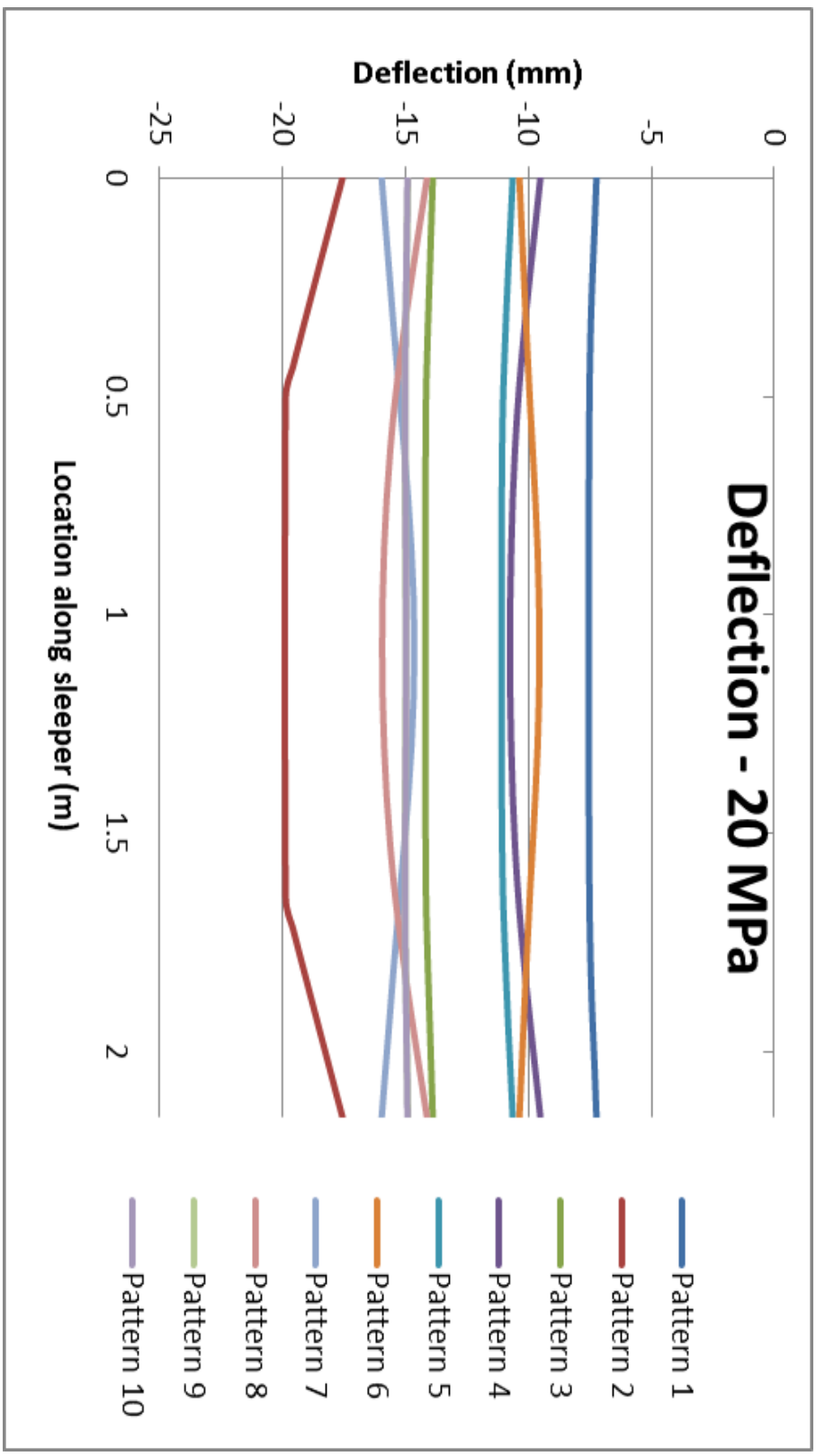
Figure 3.15: Deflection Us 20 MPa

43
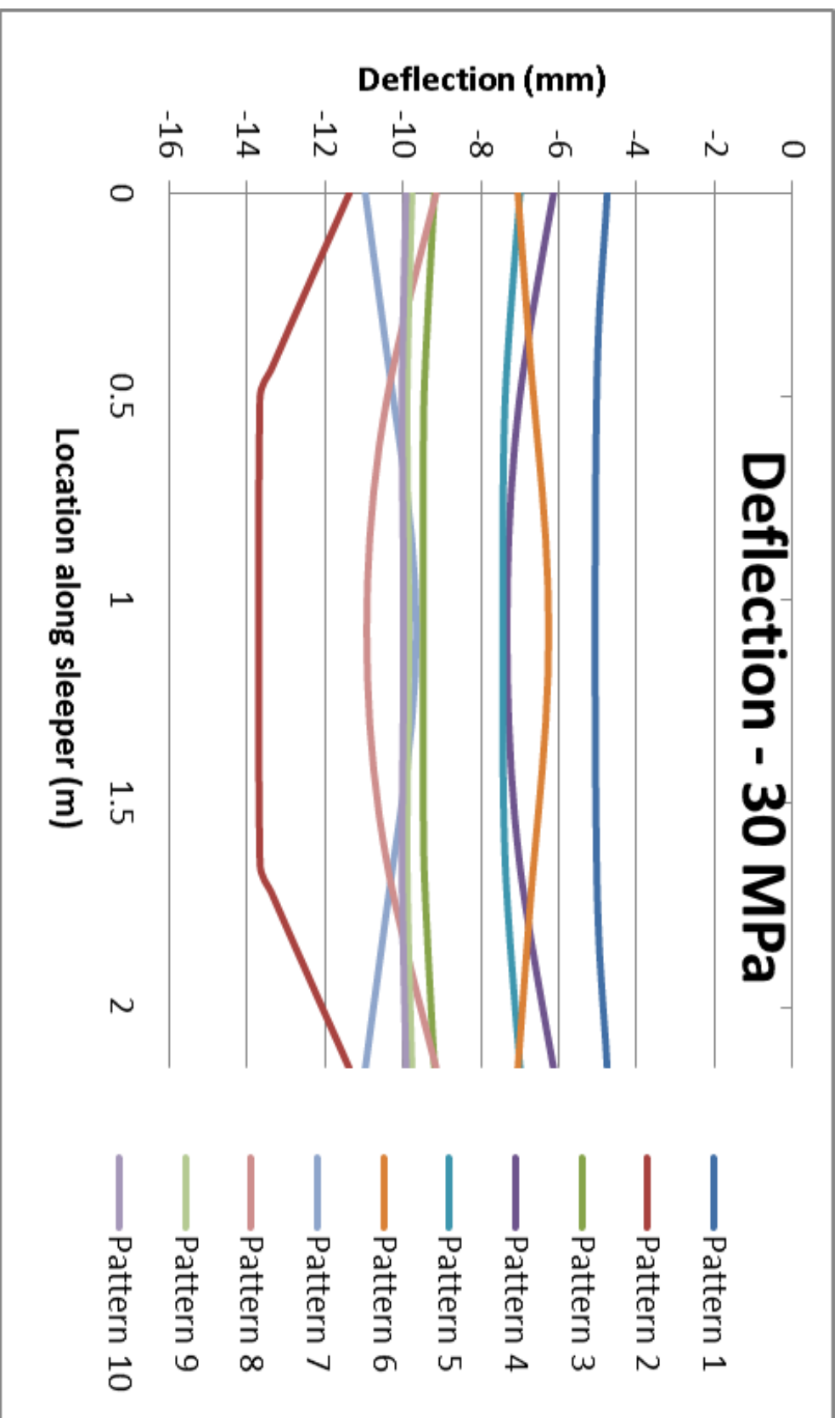
Figure 3.16: Deflection Us 30 MPa.

44
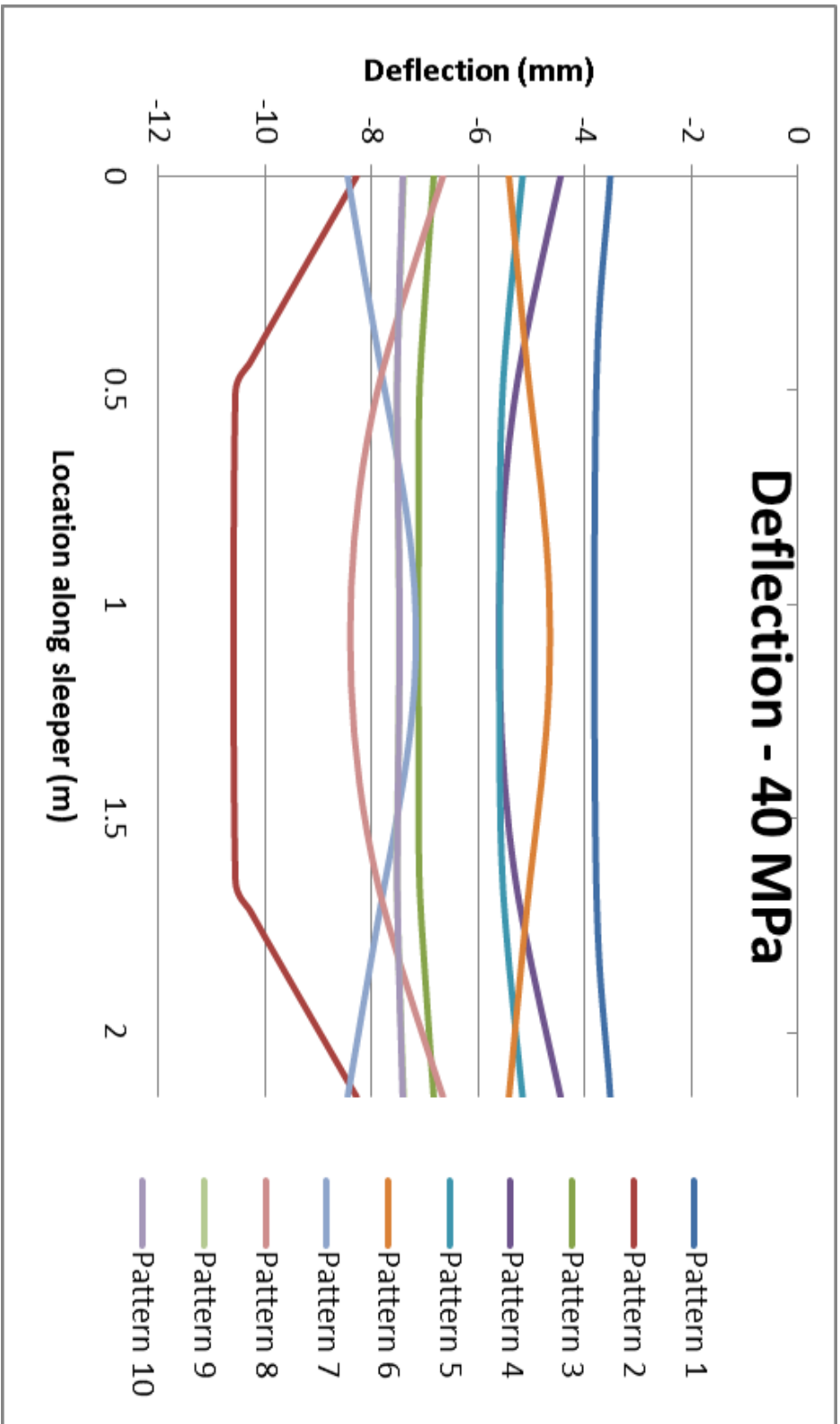
Figure 3.17: Deflection Us 40 MPa.

3.5   Conclusion

The objective of this chapter was to compare and evaluate the existing theoretical bearing pressure distribution patterns used to calculate the design bending moment and shear forces that sleepers are subjected to due to rail loading and determine which pattern will give the most conservative design forces for the next stage of the analysis. The patterns available from published literature have been analysed in strand7 and the results have been discussed above. The main findings from this stage of the study include:

- Pattern 2 will give the highest design positive bending moments and shear forces.

- Pattern 7 will give the highest design negative bending moment.

- AS1085.14 design positive rail seat and positive centre bending moments most closely match pattern 4.

- AS1085.14 negative centre bending moments most closely match pattern 6 and 7.

The chosen patterns 2 and 7 will be used for the next chapter to perform parametric studies and determine the combination of parameters which give the highest design forces, which will then be sued to design the arrangement of GFRP reinforcement.

CHAPTER 4   Parametric Study

4.1   Chapter Overview

Stage 2 involves undertaking a parametric study to determine the maximum design forces the concrete railway sleeper will be subjected to. To achieve this, the two chosen patterns from chapter 3 will be re analysed in Strand7, once again using typical support modulus values of 10 MPa, 20 MPa, 30 MPa and 40 MPa, this time with varied characteristic compressive strength values. Pattern 1 will also be re analysed with the varying parameters to allow a comparison with the Beam on Elastic Foundation results and to verify the Strand7 results are accurate.

The results of this section will provide the combination of pattern, support modulus and characteristic compressive strength of concrete which will give the highest positive and negative bending moments and shear force. From this the required reinforcement for both GFRP and steel alternatives can be determined and then the behaviour of the different concepts can be compared through finite element analysis.

4.2   Parameters

The parametric study involves varying the bearing pressure distribution patterns, the support modulus and the characteristic compressive strength. The 10 different hypothetical bearing pressure distribution patterns (Table 3.1) were analysed as a part of the first stage and from this patterns 2 and 7 were chosen for this stage of the study. Pattern 1 is also considered in this stage as a verification tool because the analytical solution only considers this support condition. Further to this the same typical support modulus values of 10 MPa, 20 MPa, 30 MPa and 40 MPa are used in this chapter.

The new parameter introduced for this stage of the analysis is concrete characteristic compressive strength (f'c). The first stage of the analysis considered a Young's modulus value of 30 GPa which correlates to f'c = 32 MPa according to AS3600 Concrete Structures (2012). For this stage two additional f'c values of 25 MPa and 50 MPa will be considered. These compressive strength values are input into Strand7 through the corresponding Young's modulus (E_c), which can be seen in Table 4.1 (AS3600, 2012).

f_c' (MPa)	20	25	32	40	50	65	80	100
f_{cmi} (MPa)	22	28	35	43	53	68	82	99
E_c (MPa)	24 000	26 700	30 100	32 800	34 800	37 400	39 600	42 200

To perform this parametric study, the existing Strand7 files were modified to incorporate the new E_c values, while keeping the rest of the model the same as described in chapter 3. The parameter values considered for this analysis are presented in Table 4.2.

Table 4.2: Parametric study values.

Parameter	Values
Patterns	1,2,7
Us (Mpa)	10, 20, 30, 40
f'c (Mpa)	25, 32, 40
Ec (Mpa)	26 700, 30 100, 34 800

4.3   Parametric Study Results

4.3.1   Strand7 Results

The Strand7 results of the parametric study for patterns 1, 2 and 7 have been tabulated below (Tables 4.3 – 4.5) with only the maximum positive and negative bending moments, shear force and deflections recorded.

	Pattern 1												
	f'c (Mpa)												
	25				32				50				
	Us (Mpa)				Us (Mpa)				Us (Mpa)				
	10	20	30	40	10	20	30	40	10	20	30	40	
M + (kN.m)	18.9273	18.7799	18.6464	18.5246	18.944	18.811	18.689	18.577	18.9639	18.8466	18.7382	18.6376	
M - (kN.m)	5.21382	5.43438	5.62733	5.79713	5.1876	5.3884	5.5664	5.725	5.15795	5.33545	5.49528	5.63974	
V (kN)	84.9781	85.2946	85.5717	85.8156	8.494	8.5228	8.5484	8.5712	84.8979	85.1526	85.382	85.5895	
Defl (mm)	14.9545	7.512	5.03084	3.79003	14.95	7.504	5.023	3.783	14.9381	7.49588	5.01492	3.7743	

Table 4.3: Pattern 1 Strand 7 Results.

	Pattern 2											
	f'c (MPa)											
	25				32				50			
	Us (MPa)				Us (MPa)				Us (MPa)			
	10	20	30	40	10	20	30	40	10	20	30	40
M+ (kN.m)	46.3797	46.0253	45.6768	45.3342	46.419	46.103	45.791	45.484	46.4631	46.1895	45.9195	45.653
M- (kN.m)	0	0	0	0	0	0	0	0	0	0	0	0
V (kN)	160.708	160.708	160.708	160.708	160.71	160.71	160.71	160.71	160.708	160.708	160.708	160.708
Defl (mm)	38.2997	20.0219	13.8132	10.7032	38.47	19.58	13.66	10.55	3.82913	19.6931	13.4891	10.3838

Table 4.4: Pattern 2 Strand 7 Results.

Pattern 7

	f'c (Mpa)												
	25				32				50				
	Us (Mpa)				Us (Mpa)				Us (Mpa)				
	10	20	30	40	10	20	30	40	10	20	30	40	
M + (kN.m)	6.14263	6.28683	6.4259	6.56011	6.126	6.256	6.381	6.502	6.1083	6.22036	6.32932	6.43531	
M- (kN.m)	33.0428	32.5587	32.091	31.6387	33.1	32.664	32.244	31.836	33.1578	32.782	32.4159	32.0593	
V (kN)	124.237	123.563	122.911	122.281	124.31	123.71	123.124	122.56	124.398	123.874	123.364	122.867	
Defl (mm)	31.064	16.0782	11.0692	8.5549	30.94	15.96	10.96	8.445	30.8035	15.8266	10.826	8.31967	

Table 4.5: Pattern 7 Strand 7 Results.

4.3.2   Strand 7 Model Verification

It is important that these Strand7 results are verified to give confidence in any conclusions
that will be made. To verify this model for the changed parameters, the results of pattern 1
will be compared to the analytical results obtained for the same pattern utilising the Beam
on Elastic Foundation (BOEF) solution (Section 2.5). The results of the BOEF solution for
the new f'c values 25 MPa and 50 MPa are presented in Table 4.6 and 4.7 respectively.

Table 4.6: Analytical Results for f'c = 25 MPa.

Analytical Results f'c = 25 MPa				
Us (Mpa)	10	20	30	40
M A-C (kN.m)	18.92755	18.78031	18.647	18.52539
M centre (kN.m)	-5.21345	-5.43372	-5.62646	-5.79611
Defl (mm)	12.47617	6.006173	3.932045	2.921498

Table 4.7: Analytical results for f'c = 50 MPa.

Analytical Results f'c = 50 MPa				
Us (Mpa)	10	20	30	40
M A-C (kN.m)	18.9639	18.84661	18.73824	18.63764
M centre (kN.m)	-5.15795	-5.33545	-5.49528	-5.63974
Defl (mm)	12.66331	6.089713	3.976621	2.946311

Comparing the Analytical results from the BOEF solution to the Strand 7 Results indicates
that the results obtained are quite accurate. The maximum positive moment is the most
accurate with the highest variation between the two methods of 0.004 %, while the negative
bending moment results were also very accurate with a maximum difference of 0.007%
occurring for Us 10 MPa and f'c of 25 MPa. Finally, the deflection values calculated in the
Strand 7 model were approximately 18 – 30% higher than the analytical solution. This large
variation in the deflection values was considered to be acceptable as the model is more
conservative and also the bending stresses are the more critical output for investigating the
suitability of the sleeper design.

4.3.3   Results and Discussion

The effect of the different patterns has been covered in detail in chapter 3, but it is again clear that the assumptions made about the distribution of bearing pressure along the sleeper for patterns 2 and 7 produce high positive and negative bending moments respectively.

 The effects of changing the support modulus have been compared in stage 1 of the analysis and again for this stage as a part of the parametric study. The comparison of loading for different support modulus allows the sensitivity of this parameter to be evaluated. From the above results it is evident that the variation in support modulus does not have a significant impact on the design forces that the sleeper will experience, it only affects the amount of deflection that occurs due to the rail loading. This is expected as the increase in support modulus doesn't increase the area that supports the load it simply offers increased resistance to settlement of the sleeper into the ballast.

These results differ from the parametric study by Manalo et.al (2012), which recorded a 15% reduction of bending moment for change in support modulus from 10 to 40 MPa assuming a uniform bearing pressure consistent with pattern 1. In comparison, for pattern 1 the average reduction for the bending moment experienced by the sleeper for increased support modulus from 10 to 40 MPa was approximately 2%. This could be due to the difference in the sleeper lengths which mean an increase in support modulus would have a greater improvement on the sleeper with a larger support area. The significantly lower sleeper modulus of 1 to 10 GPa for the fibre composite compared to the concrete sleeper modulus of approximately 30 GPa would also reduce the effect of increasing the support modulus. From this comparison it is inferred that the insignificant effect of the support modulus on the design forces is reasonable for the concrete sleeper adopted for this analysis.

One of the requirements for a concrete railway sleeper is that the longitudinal straightness of the sleeper is within 6mm. This requirement will only be considered for pattern 1 as this is the expected normal service support condition, while patterns 2 and 7 are only considered for the worst case condition for strength considerations. From the Strand 7 results for pattern 1 it can be seen that only cases with Us 30 MPa and 40 MPa meet the requirement of < 6mm deflection, therefore only these support modulus values will be considered for the next stage.

It can be seen from the results that the change in characteristic compressive strength has an insignificant effect on any of the design loads or the deflection of the sleeper. This is due to the increase in stiffness of the concrete not dramatically changing the behaviour of the

sleeper under loading and because it does not improve the support conditions. This result is different to the 75% increase in bending moment calculated by Manalo et.al (2012) for sleeper modulus increase from 1 to 10 GPa. This significant difference is believed to be due to the much higher concrete sleeper modulus values compared to the fibre composite sleeper. The high modulus of the concrete in comparison to the rail seat load means that the deflection of the sleeper and the design loads are not significantly affected by the increase in compressive strength.

Taking into consideration only support modulus 30MPa and 40 MPa and patterns 2 and 7, it is determined that the maximum positive bending moment is 45.9 kN.m from pattern 2 and the maximum negative bending moment is 32.4 kN.m from pattern 7, both with U_s = 30 MPa and f'c = 50 MPa. The maximum shear force can also be seen to be 160.7 kN from pattern 7 for all combinations of parameters.

4.4   Conclusion

The aim of this chapter was to undertake a parametric study and determine the combination of bearing pressure distribution pattern, support modulus and concrete character compressive strength that would produce the highest design forces. The main findings of this chapter are presented below:

- Support modulus values of 10 MPa and 20 MPa will not be considered as they do not meet the Australian Standard deflection requirements for a concrete sleeper.
- Characteristic compressive strength of concrete does not have a significant effect on the performance of the sleeper.
- Maximum design forces were determined as: M^+ = 45.9 kN.m, M^- = 32.4 kN.m and SF = 160.7 kN for U_s = 30 MPa and f'c = 50 MPa.

These design forces and parameters will now be used to determine the amount of reinforcement required for both GFRP and steel reinforced sleeper designs. Once the arrangement of reinforcement is determined the two sleeper types will be compared through 3dimensial finite element modelling.

CHAPTER 5   Evaluation of Behaviour of Concrete Sleeper
with GFRP Reinforcement

5.1   Chapter Overview

This stage of the project involves combining the chosen critical combination of bearing pressure distribution, support modulus and characteristic compressive strength and the resulting design forces to determine the required reinforcement for both steel and GFRP alternatives. Adopting an f'c value of 50 MPa and a typical cross section of a narrow gauge concrete sleeper, the longitudinal tensile reinforcement required for both materials was calculated and the Shear capacity of the sleeper checked.

A Finite Element Model (FEM) of both designs was then created based on the chosen layout of reinforcement. From the results of the FEM analysis a load deflection relationship was determined for each sleeper alternative which allows a comparison of the designs and ultimately allows the behaviour of the GFRP reinforced concrete sleeper to be evaluated.

5.2   Sleeper Parameters

Before the reinforcement could be determined the sleeper cross section had to be chosen and the amount of concrete cover decided. As this project considers a Queensland concrete railway sleeper, a typical narrow gauge sleeper cross section was adopted; this can be seen in figure 5.1.
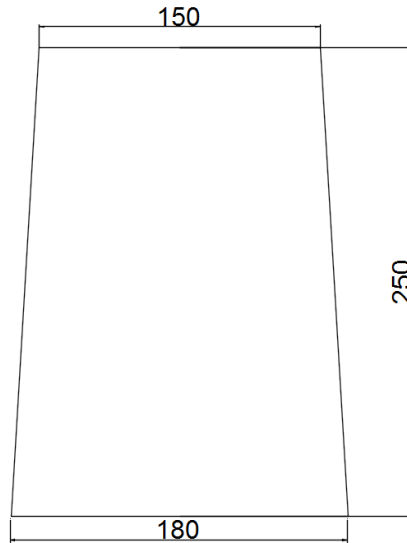
Figure 5.1: Typical cross section adopted for this analysis.

For this study a typical value of 38mm from the outer face of the sleeper to the centroid of the outermost reinforcement was chosen (Murray, 2015). This value is acceptable based on the minimum cover requirements of AS3600 (2009). 50 MPa concrete is used for both sleeper designs and considering the sleeper as exposure classification B1, the required cover is 25mm. Therefore, bars up to 26mm in diameter can be used and still satisfy this requirement.

5.3   Steel Reinforcement Design

The amount of steel reinforcement required to ensure the concrete sleeper can withstand the design forces ($M^+ = 45.9$ kN.m, $M^- = 32.4$ kN.m and SF = 160.7 kN) will be determined in accordance with Sections 8. 1 and 8.2 of AS3600 (2009). Details on the determination of flexural and shear reinforcement are provided in the proceeding sections.

5.3.1   Flexural Strength

When determining the required reinforcement, the stress strain pattern for the sleeper must first be clarified. The stress strain diagrams in figure 5.2 below show the variation of stress and strain due to an applied moment, with the natural axis defining the boundary between compressive and tensile stress. In accordance with AS3600 section 8.1, the compressive strain is limited to 0.003 at the extreme compression fibre, with the stress/strain linearly distributed. To simplify the analysis, the compressive stress is converted to an equivalent uniform rectangular stress block. The stress block is bounded by the sides of the cross section and a line parallel to the neutral axis at a distance γdn from the extreme compressive fibre.
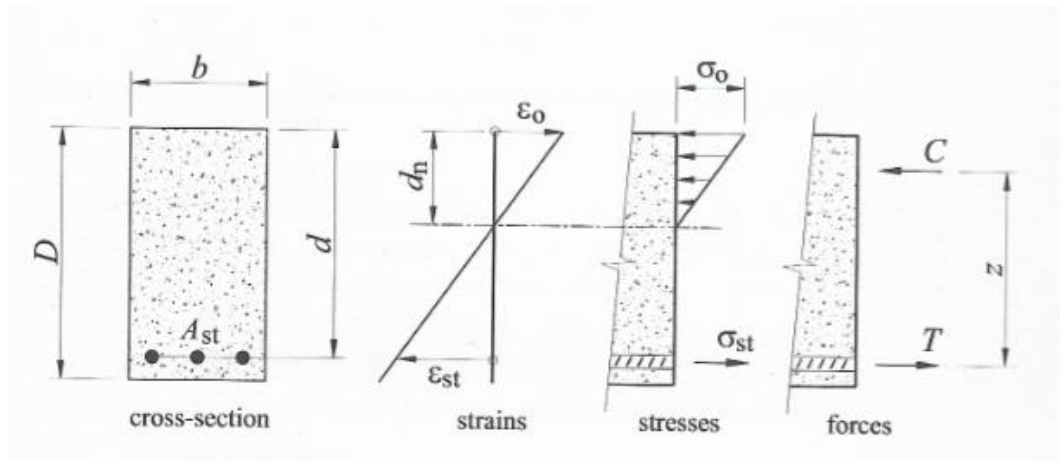
Figure 5.2: Stress strain relationship of concrete section due to applied moment.

$$\gamma = 1.05 - 0.007f'c \ (0.67 \le \gamma \le 0.85) \qquad (5.1)$$

$$\gamma = 1.05 - 0.007 \ x \ 50 \ MPa = 0.7 \ (Within \ limits \ 0.67 \le \gamma \le 0.85)$$

The function of neutral axis depth to effective depth is described by equation 5.2. Where k_u is limited to 0.36 to ensure a ductile section, therefore this limiting value will be adopted for this design.

$$d_n = k_u \ d \qquad (5.2)$$

$$d_n = k_u \ d = 0.36 \ x \ 212mm = 76.32mm$$

With the neutral axis determined, the required tensile reinforcement to meet the design bending moments can be calculated. The Moment capacity of the section can be described by $M = Tz$, where T is the tensile force and z is the moment lever arm as depicted in figure 5.2.

To meet the strength requirements, the reduced section moment capacity must be greater than or equal to the design moment. The capacity reduction factor ϕ, is a function of k_u as described in equation 5.3.

$$\phi = 1.19 - 13\,k_{uo}/12 \tag{5.3}$$

$$\phi = 1.19 - 13\ x0.36/12 = 0.8$$

Therefore, the required moment capacity is:

$$Mu = M*/\phi \tag{5.4}$$

Therefore:

$$Mu+ = 45.9\ kN.m/\ 0.8 = 57.4\ kN.m$$

$$Mu- = 32.4\ kN.m/\ 0.8 = 40.5\ kN.m$$

The resultant compression force is approximated to occur at the midpoint of the stress block. As the width of the sleeper changes slightly throughout the depth of the section, this would not be the exact location of the centroid but is accurate enough for this purpose. With this information and assuming only one layer of reinforcement for both positive and negative bending, the moment capacity can be described (Eq. 5.5) and rearranged to find the required area of steel reinforcement (Eq. 5.6).

$$Mu = Tz = A_{st}\ f_y \left(d - \frac{\gamma d_n}{2}\right) \tag{5.5}$$

$$\therefore A_{st} = \frac{Mu}{fy\left(d - \frac{\gamma d_n}{2}\right)} \tag{5.6}$$

The calculated area of reinforcing was then converted to the equivalent required number of bars. The required quantity of R6, N10, N12, N16 and N20 bars were calculated, to determine the most suitable bar size for the sleeper cross section. The varying yield strengths of the different bar types had to be considered, with these values shown in table 5.1.

Table 5.1: Bar types and their corresponding yield strength.

Bar Type	Yield Strength f_y (MPa)
R6	250
N10	500
N12	500

N16	500
N20	500

Using these values the number of bars required was calculated and rounded up to the nearest whole bar. These results can be seen in table 5.2.

Table 5.2: Required Steel Tensile Reinforcement.

Bar Type	**Bottom Bars Required**	**Top Bars Required**
R6	44	33
N10	8	6
N12	6	5
N16	4	3
N20	2	2

From the results it can be seen that R6 up to N12 bars are unrealistic for the section considering the large number of bars and the limited sleeper width of 180mm. From the remaining bar sizes, it was determined that using 2 N20 bars would be the best design as placing 4 bars into the section would limit the spacing between the bars which could cause issues in proper distribution of the concrete through the section.

5.3.2 Shear Strength

The shear reinforcement requirements of the section in supporting the 160.7 kN design load were checked in accordance with section 8.2.7.1 of AS3600 (2009). The ultimate shear strength of the sleeper without shear reinforcement was first checked using equation 5.7. The shear capacity must be greater than or equal to the design shear force divided by a capacity reduction, with the capacity reduction factor for shear of 0.7. The calculations below demonstrate that no shear reinforcement is needed for the sleeper section. The resulting configuration for the concrete sleeper with steel reinforcement can be seen in figure 5.3.

$$Vuc \; = \; \beta_1 \, \beta_2 \, \beta_3 \, b_v \, d_o \, f_{cv} \left(\frac{A_{st}}{b_v \, d_o} \right)^{1/3} \hspace{4cm} (5.7)$$

Where:

$$Vuc = \frac{V^*}{\varphi} = \frac{160.7}{0.7} = 229.6 \, kN$$

$$\beta1 = 1.1(1.6 - \frac{d_o}{1000}) \geq 1.1 \tag{5.8}$$

$$\beta1 = 1.1\left(1.6 - \frac{212}{1000}\right) = 1.527 \geq 1.1$$

$$\beta2 = \beta3 = 1$$

$$bv = bave = 162.7mm$$

$$fcv = f'c^{\frac{1}{3}} \leq 4MPa \tag{5.9}$$

$$fcv = 50^{\frac{1}{3}} = 3.68 \, MPa \leq 4MPa$$

$$Ast = 628.3mm^2$$

$$\therefore Vuc = 1.527 \times 1 \times 1 \times 162.7 \times 3.68 \times \left(\frac{628.3}{162.7 \times 212}\right)^{1/3} = 240.6 \, kN > 229.6 \, kN$$
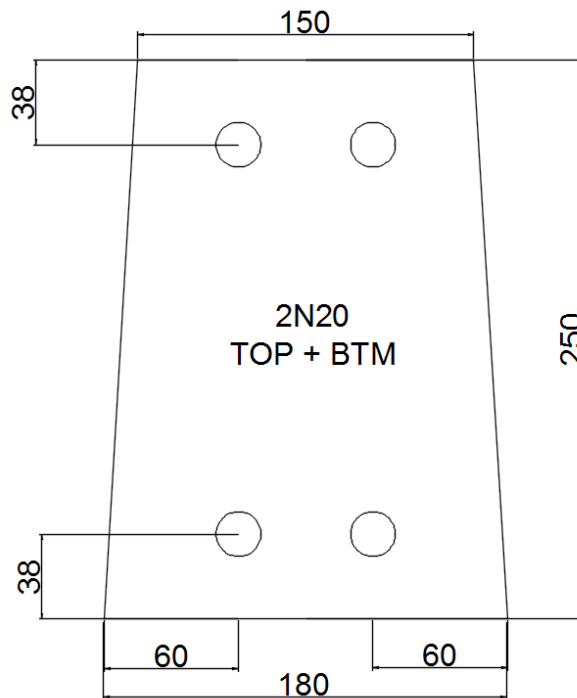
Figure 5.3: Steel reinforcement layout.

5.4   GFRP Reinforcement Design

The amount of GFRP reinforcement required so the sleeper can withstand the design forces (M^+ = 45.9 kN.m and M^- = 32.4 kN.m) will be determined in accordance with Section 8 of CSA S806-12 (2012), Design and construction of building structures with fibre-reinforced polymers. The design procedure for flexural strength is provided in the following sections.

5.4.1   Flexural Strength

The design philosophy for GFRP reinforcement is very similar to that of AS3600, with a rectangular stress block assumed and a linear stress strain relationship. One difference in the methods is that the GFRP standard considers a maximum concrete strain at the extreme compression fibre of 0.0035 instead of 0.003. This design philosophy is depicted in figure 5.4.
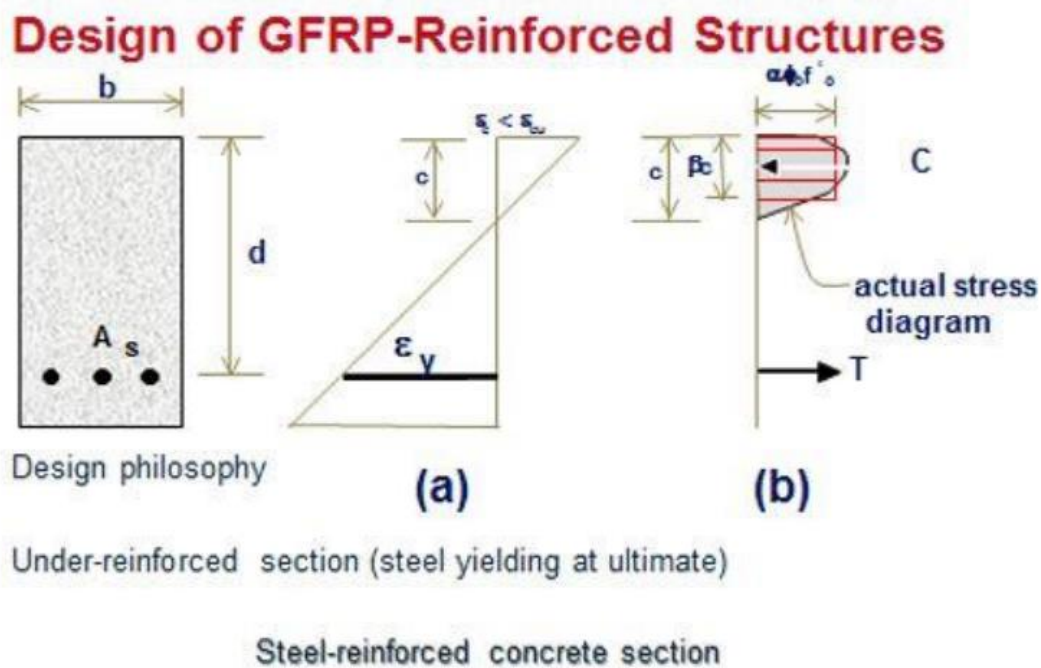
Figure 5.4: Design of GFRP reinforced structures (V-ROD Australia, 2011).

The method followed to determine the moment capacity of the sleeper is essentially the same as for steel with some different characters used. Instead of γd_n the terms $\beta_1 c$ is used, with c being the neutral axis depth. The factor β_1 is equal to:

$$\beta_1 = 0.97 - 0.0025 f'c \geq 0.67 \tag{5.10}$$

$$\beta_1 = 0.97 - 0.0025 \times 50 = 0.845 \geq 0.67$$

The capacity factor applied to GFRP reinforcement is $\phi_F = 0.65$. Therefore, the required moment capacity is:

$$Mu = M^*/\phi_F \tag{5.11}$$

Therefore:

$$Mu+ = 45.9 \, kN.m/ \, 0.65 = 70.6 \, kN.m$$

$$Mu- = 32.4 \, kN.m/ \, 0.65 = 49.8 \, kN.m$$

The resultant compressive force is again approximated to occur at the midpoint of the stress block and the reinforcement is designed assuming one layer top and bottom. The neutral axis depth is taken as 0.36d to allow a consistent comparison. With this information the moment capacity can be described (Eq 5.12) and then rearranged with A_{st} as the unknown (Eq. 5.13).

$$Mu = Tz = A_{st} \, f_u \left(d - \frac{\beta_1 c}{2} \right) \tag{5.12}$$

$$\therefore A_{st} = \frac{Mu}{fu \left(d - \frac{\beta_1 c}{2} \right)} \tag{5.13}$$

A requirement of the design standard limits the tensile strength used in the design of GFRP reinforcement to 25% of the minimum guaranteed tensile strength. This is due to the low modulus of the GFRP material, which at the ultimate tensile strength would produce significant cracking of the concrete as it elongates, leaving the sleeper unusable. For this analysis 5 different sized 60 GPa V- Rod GFRP bars were chosen. The parameters for each bar type are displayed in table 5.3.

Table 5.3: GFRP bar properties (V- ROD, 2012).

Bar Size	Bar Diameter (mm)	Min Guaranteed f_u (MPa)	25% Min Guaranteed f_u (MPa)
#3	9.53	1372	343
#4	12.7	1312	328
#5	15.875	1184	296
#6	19.05	1105	276.25
#7	22.225	1059	264.75

Using these parameters, the area of GFRP reinforcement required and subsequently the number of bars required was calculated. The results of these calculations can be seen in table 5.4.

Table 5.4: Required GFRP Tensile Reinforcement.

Bar Size (mm)	Bottom Bars Required	Top Bars Required
9.53	17	12
12.7	10	7
15.875	7	5
19.05	5	4
22.225	4	3

The results indicate that only the 22mm nominal diameter bar is suitable to fit into the cross section and still provide acceptable spacing between bars while maintaining concrete cover. The reduction in tensile strength with increasing bar diameter is potentially problematic for designing smaller sections where space in the section is limited. It was considered that 4 bars in the bottom face would be too congested so 3 bars were chosen for the outermost layer with another layer above containing 2 22mm bars. This design was again checked against the design bending moment and met the flexural capacity requirements. The final chosen design can be seen in figure 5.5.
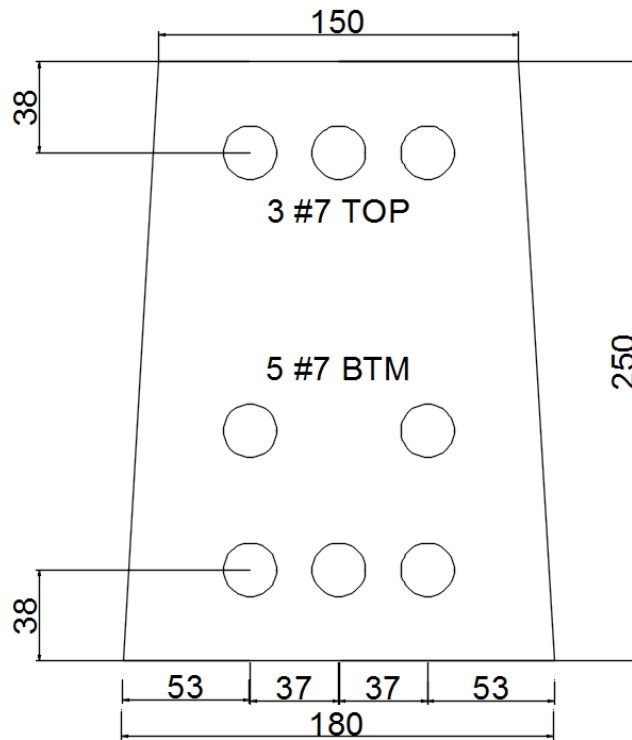
Figure 5.5: GFRP reinforcement layout.

5.5   Finite Element Analysis

5.5.1   Model Development

The first step in the FEA was to set up the 2dimensional model of each sleeper based on the designs in the previous sections. The first step involved creating nodes at all corners, reinforcement bar centroids and locations where the centre lines of the bars meet the perimeter of the sleeper. These nodes were placed in the XY plane. Also as the steel reinforced sleeper is symmetrical only one half was initially modelled.

Next nodes were created so that there were four equal square plate elements forming the location of each reinforcing bar. An example of this can be seen in Figure 5.6. The holes where the reinforcement is placed were then created using the grading function in strand7, the end result for the GFRP sleeper is illustrated in figure 5.7.
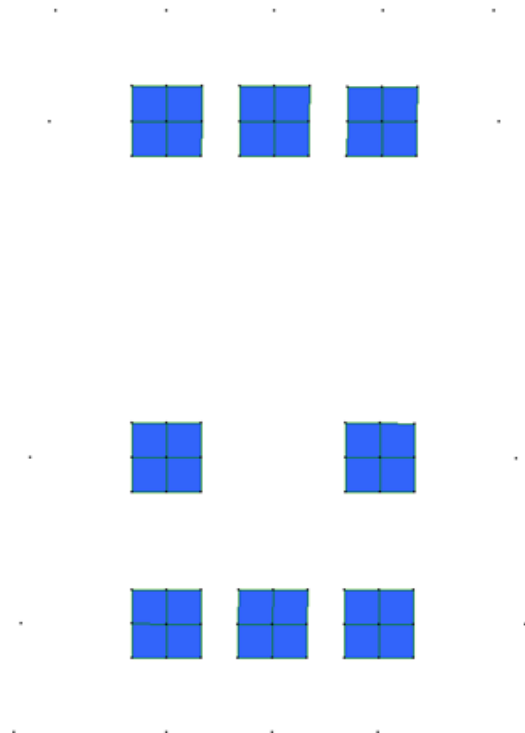
Figure 5.6: GFRP model with square elements to create reinforcing bar locations.
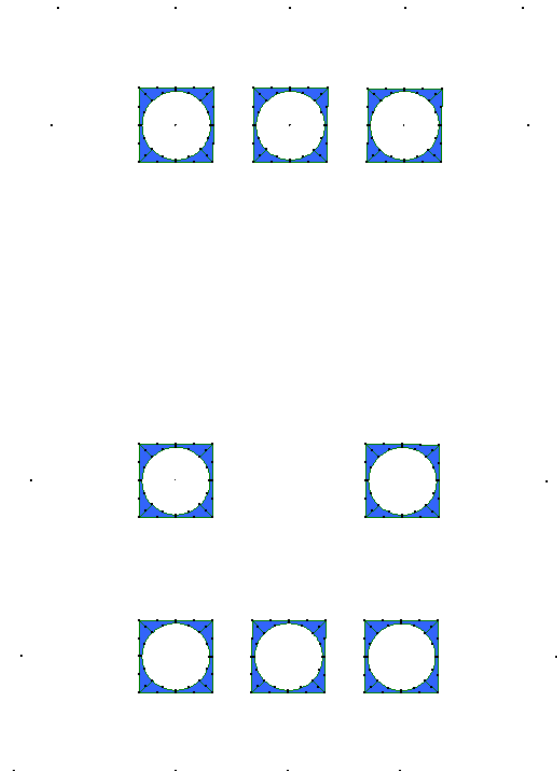
Figure 5.7: GFRP model with reinforcing bar holes created.

The next step was to create the remaining plates for the concrete section and then to create a new plate property and model the reinforcement. The reinforcement bar was approximated by square quad 8 elements which have the capacity for nonlinear edges. To approximate the circle shape the intermediate nodes of the square elements were moved to the corresponding circle circumference nodes. This same process was followed for both sleeper designs, with the GFRP reinforced sleeper at this stage displayed in figure 5.8.
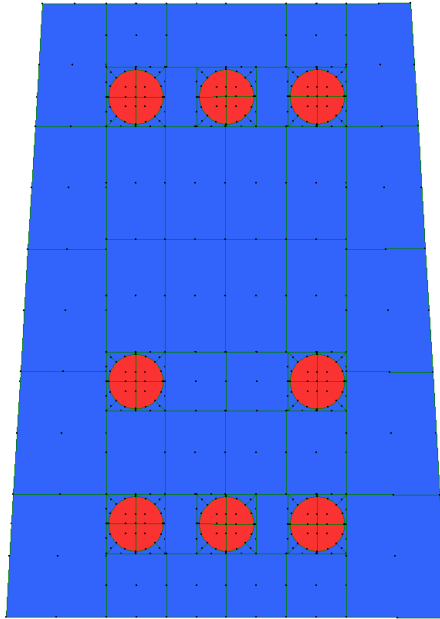
Figure 5.8: Complete plate model for GFRP reinforced sleeper.

The next step was to use the extrude tool in strand 7 to extend the plate the total sleeper length of 2.15m in the Z direction. This then creates the 3D model of the sleeper design, so the plate element could then be selected and deleted. From here the brick point load function was used to apply the 160 kN rail seat load at the rail location, by selecting the top centre brick element and manually inputting the coordinates of the two rail loads. After this the nodes on the end faces of the sleepers were selected and the sleeper restrains were created. To model the behaviour of the sleeper in railway conditions the translation in the X and Z directions were fixed, only allowing the sleeper to move up and down. The nodes were also fixed for rotation in the Y and Z axis. Finally, the support modulus was included in the model by selecting the brick faces on the bottom of the sleeper and applying the face support function. This was set to 30 MPa and only for compression. An example of the setup steel reinforced model is shown in figure 5.9.
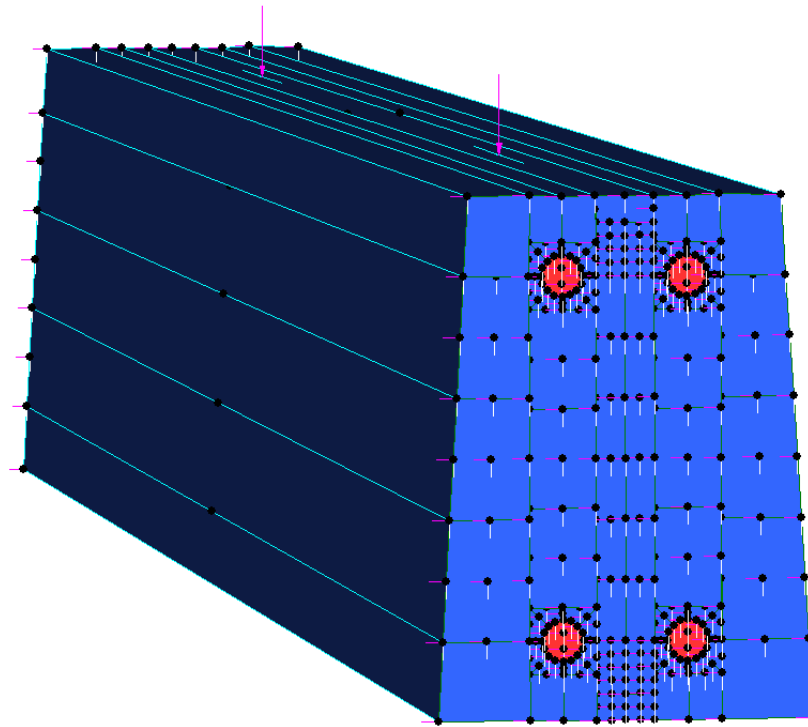
Figure 5.9: Setup model for steel reinforced concrete sleeper.

Both models were then subdivided to increase the accuracy of the model. The GFRP reinforced sleeper was subdivided into 29475 bricks while the steel reinforced model was subdivided into 20474 bricks. The higher number of bricks for the GFRP model is because there are more bars modelled creating a more complicated initial sleeper end face plate.

Before the FEA could be performed the brick properties for each material had to be set. For concrete and steel the material properties in the Strand7 library were used while for the GFP bars the V- ROD specification sheet data was used. The property input values for each material have been tabled below.

Table 5.5: Material input properties for Strand 7.

	50 MPa Concrete	**Steel**	**GFRP**
Modulus (MPa)	38,000	200,000	62,600
Poisson's Ratio	0.2	0.25	0.26
Density (kg/m³)	2400	7870	2980
Thermal Expansion (/K)	1.0×10^{-5}	1.15×10^{-5}	6.2×10^{-6}

With the model setup and all required parameters set the model could then be run. For this project a nonlinear static analysis was performed with 10 load increments of 10% applied from 0 – 160 kN.

5.6   Results and Discussion

From the results the location of the maximum deflection was found for both the steel reinforced sleeper and the GFRP reinforced sleeper and then the deflection data for each increment at these critical nodes was recorded. This data was then transferred into excel and the load deflection behaviour of both sleeper concepts was graphed to allow a comparison of the structural behaviour. Figure 5.10 shows this relationship.
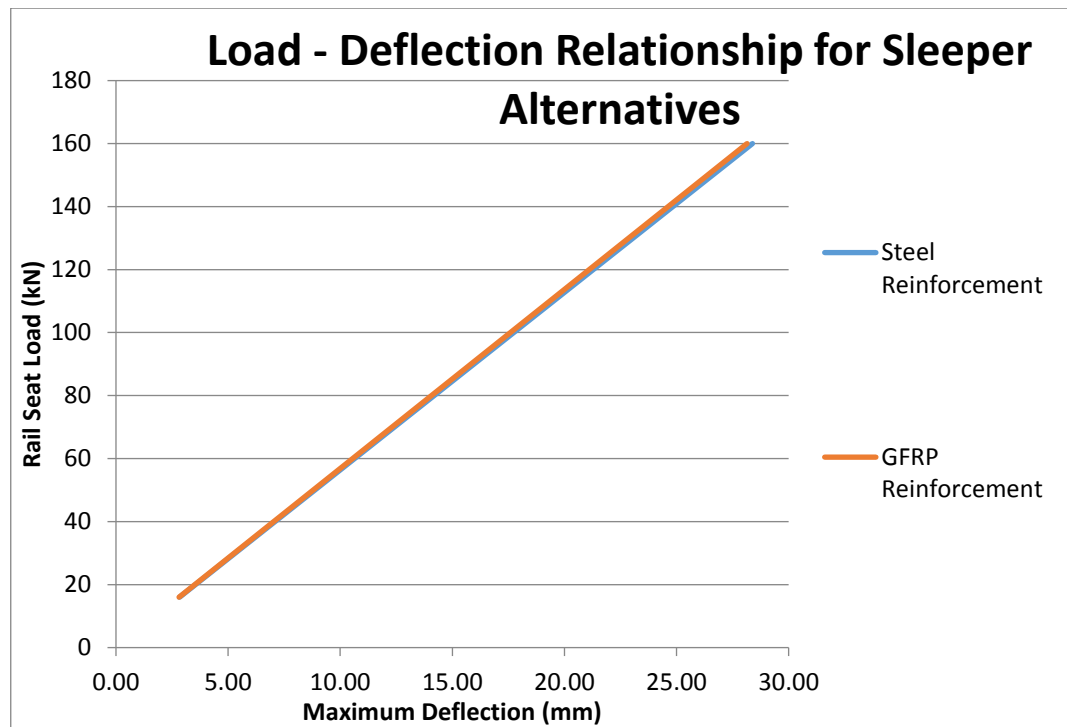
Figure 5.10: Load- deflection relationship for alternative sleeper designs.

The results displayed in figure 10 indicate that both the GFRP reinforced sleeper and the steel reinforced sleeper have almost identical deflection for increasing rail seat load up to the design load of 160.7 kN. This indicates that the GFRP design performs just as well as the traditional steel reinforced concrete sleeper for a 25 tonne axle load and narrow track gauge.

The deformed shape of both GFRP reinforced and steel reinforced sleepers can be seen in figures 5.11 and 5.12 respectively. From this it can be seen that the deformed shape of both sleepers under the design rail seat load match and approximate the expected sleeper deflected shape. This indicates that the result of the two models is as expected and allows

them to be compared with confidence. A potential point of poor representation of the real behaviour of the model could be due to the rail seat load being modelled as a point load where in reality it would be spread evenly over the rail pad. This is highlighted in both models by the excess compression of the concrete on the top face, under the point load.

This similarity in performance suggests that the design methods for GFRP are quite accurate in their assumed reduction factors and the reduced design tensile strength. The maximum stress in the GFRP reinforcement and steel reinforcement are 164 MPa and 384 MPa respectively. This suggests that the sections are well below their ultimate strength capacity and that both designs would be suitable for use as railway sleepers based on strength considerations. The fact that the stress in the GFRP is 57% lower is as expected due to the extra reinforcement and it is concluded that the GFRP sleeper would also meet the serviceability requirements.

In saying this there is approximately 54% more area of reinforcement in the GFRP reinforced sleeper. This could indicate increased costs of materials and production of this potential design, in comparison with steel reinforced sections. Therefore, this indicates the need for further study on this topic, including full scale experimental testing on the structural behaviour and durability properties of this design. From the results of that testing a cost analysis could be performed to determine whether the implementation of this design is suitable.
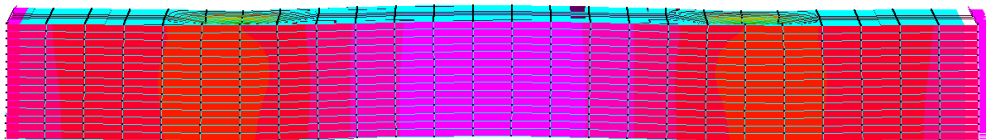
Figure 5.11: Deformed shape of the GFRP reinforced concrete sleeper.
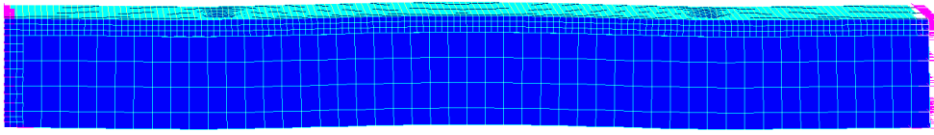
Figure 5.12: Deformed shape of the steel reinforced concrete sleeper.

5.7   Conclusion

The objective of this chapter was to combine the critical parameters and design loads determined in the previous chapters to design the layout of both steel and GFRP reinforcement for the narrow gauge sleeper. A finite element model was then created for each sleeper alternative to evaluate the performance of this new sleeper concept. The main findings of this chapter include:

- Concrete sleeper required 2 N20 bars top and bottom for steel reinforcement.

- Concrete sleeper required 3 #7 bars top and 5 #7 bars bottom for GFRP reinforcement.

- Load deflection behaviour of GFRP reinforced sleeper is equal to or better than steel alternative.

- Both steel and GFRP reinforcement alternatives meet the strength requirements.

- 54% increase in amount of reinforcement required for GFRP compared to steel.

The findings of this chapter highlight the need for further work to be done on this topic, both experimental and theoretical. This new concept is structurally adequate but needs to be proved to be financially feasible before it would be adopted for use in the railway industry.

CHAPTER 6   Conclusions and Further Work

6.1   Conclusion

Traditional sleeper materials of timber, steel and concrete are commonly not reaching their target design life, due to various failure mechanisms. This costs not only the railway industry millions of dollars each year in repair work, but also cost the environment large amounts of resources for the production of these replacement sleepers. Therefore, there is a significant need for a more durable sleeper design. This research assessed the behaviour of concrete sleepers reinforced with GFRP bars as a potential solution to this need.

In undertaking this assessment, the current proposed hypothetical bearing distribution patterns for sleepers were analysed and it was found that patterns 2 and 7 (Table 3.1) gave the highest design bending moments and shear forces. From this the critical patterns were again analysed to determine the effect of the support modulus and the sleeper modulus. The results indicating that the support modulus was only significant to the deflection of the sleeper, while the sleeper modulus had little effect on either deflection or design forces.

The critical loads and the corresponding parameters were then used to determine a suitable layout of both GFRP and steel reinforcement. The designs were then assessed using FEM analysis, with the GFRP alternative performing slightly better than steel reinforced sleeper. This indicates that the use of concrete sleepers reinforced with GFRP bars meets the ultimate strength considerations, with the drawback being the excess GFRP reinforcement required compared to steel to meet the serviceability requirements.

6.2   Future Work

There is still a lot more research required before the suitability of concrete sleepers reinforced with GFRP bars can determined. Further on from this research, full scale experimental testing on the structural behaviour of this sleeper model could be undertaken to verify the conclusions made from the theoretical analysis performed. Analysis of a wider gauge sleeper could also be undertaken to determine if GFRP reinforcement would be more suitable for larger sleepers.

Further testing could be performed on the serviceability and durability performance of this sleeper design, to quantify the benefits of this design in comparison to the sleeper materials currently used in the industry. This could also help to determine if the amount of GFRP reinforcement could be reduced, which make this sleeper design more appealing.

Finally, a cost benefit analysis of this sleeper design would need to be undertaken to demonstrate the overall benefits of this new design compared to traditional materials, which could be assessed by Railway industry for potential application of this design.

References

AREA 1975, 'Manual Recommendations, Special Committee on Concrete Ties, Part 10 Concrete Ties (and -Fastenings)', *AREA Bulletin 655*.

AREA 1985, 'Manual for Railway Engineering', *American Railway Engineering Association*, Washington D.C.

Ashour, AF 2006, 'Flexural and shear capacities of concrete beams reinforced with GFRP bars', *Construction and Building Materials*, vol. 20, no. 10, pp. 1005-1015, <http://www.sciencedirect.com/science/article/pii/S0950061805001820>

Bakharev, T, Struble, LJ 1997, 'Microstructural features of railseat deterioration in concrete ties', J Mater Civil Eng, vol.9, pp.146–153.

Canadian Standards Association 2012, Design and construction of building structures with fibre-reinforced polymers, S806-12, Canadian Standards Association, Ontario, Canada.

Clarke, CW 1957,'Track Loading Fundamentals', *The Railway Gazette*.

Ferdous, W, Manalo, A 2014, 'Failures of mainline railway sleepers and suggested remedies – Review of current practice', *Engineering Failure Analysis*, vol. 44, pp. 17-35.

González-Nicieza, C, Álvarez-Fernández, MI, Menéndez-Díaz, A, Álvarez-Vigil, AE, Ariznavarreta-Fernández, F 2008, 'Failure analysis of concrete sleepers in heavy haul railway tracks', *Engineering Failure Analysis*, vol.15, pp.90–117.

Hagaman, BR, McAlpine, RJA 1991, 'ROA timber sleeper development project' , *Conference on railway engineering: demand management of assets*, Institution of Engineers, Barton, ACT, Australia, pp. 233-237.

Hansard, A 1988, 'Rail Sleepers in Australia', *Journal of the Rail Track Association,* Australian March.

Hetenyi, M 1967, 'Beams on Elastic Foundation', The University of Michigan Press.

International Federation for Structural Concrete 2006, 'fib bulletin 37: *Precast Concrete Railway Track Systems*', state-of-the-art report.

Jeffs, T, Tew, G.P 1991, 'SLEEPERS AND BALLAST', *A REVIEW OF TRACK DESIGN PROCEDURES,* vol. 2, pp. 31-205.

Manalo, A, Aravinthan, T, Karunasena, W & Ticoalu, A 2010, 'A review of alternative materials for replacing existing timber sleepers', *Composite Structures*, vol.92, no.3, pp.603-611, <http://www.sciencedirect.com/science/article/pii/S0263822309003286>

Manalo, A, Aravinthan, T, Karunasena, W, Stevens, N 2012,'Analysis of a typical railway turnout sleeper system using grillage beam analogy', *Finite Elements in Analysis and Design,* vol. 48, pp. 1376-1391.

Mohammed, T U, Otuski, N, Hisada, M and Shibata, T 2001, 'Effect of Crack Width and Bar Types on Corrosion of Steel in Concrete', *Journal of Material in Civil Engineering*, vol. 13, pp. 194–201.

 Molded Fiber Glass Companies n.d, *Technical Design Guide for FRP Composite Products and Parts*, Molded Fiber Glass Companies, viewed 20 April 2016, <http://www.moldedfiberglass.com/sites/default/files/docs/MFG_Technical_Design_Guide_FRP_Composite_0.pdf>

Morris, A, Bland, S, Monday, I 1995,' Rail freight 1995: international benchmarking ', *Bureau of Industry Economics,* Canberra, Australia.

Murray, M 2015, 'Heavy Haul Sleeper Design – A Rational Cost – Saving Method', *IHHA 2015 Conference,* 21 -24 June 2015, Perth, Australia.

Narayanan, RS, Beeby, AW 2005, 'Designers' guide to EN 1992-1-1 and EN 1992-1-2. Eurocode 2: design of concrete structures', General *rules and rules for buildings and structural fire design*, Thomas Telford Ltd.

Neville, AM 2012, 'Properties of concrete', *England: Longman Scientific & Technical.*

ORE 1969, 'Stresses in Concrete Sleepers, Question D17, Stresses in the Rails, the Ballast and the Formation Resulting from traffic Loads', *Report D71/RP9/E*, Utrecht.

O'Rourke, MD 1978, 'Critique of Conventional Track Design Procedures as Applied to Heavy Axle Load Conditions', BHP Melb. Res. Labs Rep. No MRL/C77/78/27(1), (BHP MNM HI/TDC/78/053).

Palomo, A, Jiménez, AF, Hombrados, CL, Lleyda, JL 2007, 'Railway sleepers made of alkali activated fly ash concrete', *Revista Ingeniería de Construcción,* vol.22, pp. 75-80.

Remennikov, A & Kaewunruen, S 2005, 'Investigation of vibration characteristics of prestressed concrete sleepers in free-free and in-situ conditions', *Australian Structural Engineering Conference* 2005 (ASEC 2005), Newcastle, Australia, < http://ro.uow.edu.au/cgi/viewcontent.cgi?article=1286&context=engpapers >

Rezaie, F, Shiri, MR, Farnam, SM 2012, 'Experimental and numerical studies of longitudinal crack control for pre-stressed concrete sleepers', Engineering *Failure Analysis*, vol. 26, pp. 21-30.

 Sadeghi, J M, Youldashkhan, M 2005, 'Investigation on the accuracy of the current practices in analysis of railway track concrete sleepers', *International Journal of Civil Engineering,* vol. 3, no. 1.

Standards Australia 2012, *Concrete Structures*, AS3600, Standards Australia, Sydney, Viewed 10 August 2016,
<http://www.saiglobal.com/online/autologin.asp>

Standards Australia 2012, *Railway track material, Part 1: Steel Rails*, AS1085.1, Standards Australia, Sydney, Viewed 25 April 2016,
<http://www.saiglobal.com/online/autologin.asp>

Standards Australia 2012, *Railway track material, Part 14: Prestressed concrete sleepers*, AS1085.14, Standards Australia, Sydney, Viewed 25 April 2016,
<http://www.saiglobal.com/online/autologin.asp>

Taherinezhad, J, Sofi, M, Mendis, P A and Ngo, T 2013, 'A Review of Behaviour of Prestressed Concrete Sleepers', *Electronic Journal of Structural Engineering,* vol. 13.

Talbot, AN, (Chairman) et al 1918-1934, 'Stresses in Railroad Track, Report of the Special Committee to Report on Stresses in Railroad Track', *AREA proceedings*.

Tang, WC, Lo, TY & Balendran, RV 2008, 'Bond performance of polystyrene aggregate concrete (PAC) reinforced with glass-fibre-reinforced polymer (GFRP) bars', *Building and Environment*, vol. 43, no. 1, pp. 98-107, <http://www.sciencedirect.com/science/article/pii/S0360132306004331>

Thomas Telford 1992, 'Durable concrete structures: design guide by Comite Euro-International Du Beton'.

V-ROD Australia 2011, *Designing with V-ROD,* V-ROD Australia, viewed 25 August 2016, < http://www.vrodaustralia.com.au/wp-content/uploads/2011/07/Designing-with-V-Rod.pdf>

V-ROD Canada 2012, *V-ROD HM- 60 GPa Grade III – Oct. 2012,* V-ROD Canada, viewed 20 August 2016, < http://www.vrodcanada.com/product-data/gfrp-specification-guide>

Zhao, J, Chan, AHC & Burrow, MPN 2006, 'Reliability analysis and maintenance decision for railway sleepers using track condition information', *J Oper Res Soc*, vol. 58, no. 8, pp. 1047-1055, <http://dx.doi.org/10.1057/palgrave.jors.2602251>

Zi, G, Moon, DY, Lee, S-J, Jang, SY, Yang, SC, Kim, S-S 2012, 'Investigation of a concrete railway sleeper failed by ice expansion', *Engineering Failure Analysis*, vol. 26, pp. 151–163.

Appendix A: Project Specification

ENG4111/ 4112 Research Project

Project Specification

For: Trent Baker

Title: Analysis on the behaviour of FRP reinforced concrete railway sleepers

Major: Civil Engineering

Supervisors: Allan Manalo

Enrolment: ENG4111 – ONC S1, 2016

ENG4112 – ONC S2, 2016

Project Aim: To analyse the behaviour of precast concrete railway sleepers reinforced with glass fibre reinforced polymer (GFRP) bars and examine the suitability of this new railway sleeper concept.

Programme: Issue A, 16th March 2016

1. Research background information on the design and analysis of concrete railway sleepers.

2. Compare and evaluate the existing equations and theories for calculating the maximum positive and negative bending moment and shear forces that the sleepers are subjected to, using theoretical and Finite Element Modelling (FEM) analyses.

3. Perform parametric investigations utilising either theoretical or FEM analysis to determine the effect of important design parameters on the behaviour of precast concrete sleepers and evaluate against the performance requirements for a Queensland precast concrete railway sleeper.

4. Evaluate the structural behaviour of the precast concrete sleeper reinforced with GFRP bars and compare with the performance of an existing precast concrete sleeper reinforced with steel reinforcement, using FEM simulation.

If time and resources permit:

5. Perform full-scale experimental testing of a precast concrete sleeper reinforced with GFRP bars to verify the results of the FEM simulation.